energy&fuels

pubs.acs.org/EF

Article

Potential Application of Fe_2O_3 and Functionalized SiO_2 Nanoparticles for Inhibiting Asphaltene Precipitation in Live Oil at Reservoir Conditions

Fatemeh Mahmoudi Alemi, Seyed Ali Mousavi Dehghani, Ali Rashidi, Negahdar Hosseinpour,* and Saber Mohammadi*

Cite This: *Energy Fuels* 2021, 35, 5908−5924

Read Online

ACCESS | Metrics & More | Article Recommendations | Supporting Information

ABSTRACT: Despite the numerous works devoted to the effect of nanoparticles on asphaltene formation, their potentials for controlling asphaltene precipitation in live oils at realistic pressure−temperature conditions of oil fields have not been studied. In this study, Fe_2O_3 and functionalized SiO_2 nanoparticles were synthesized to investigate theirs effects on asphaltene precipitation and aggregation in a light live oil with a high asphaltene deposition risk. The high pressure-high temperature (HPHT) experiments including solid detection system, high pressure microscopy and HPHT filtration were designed and conducted. The results show that during depressurization of the oil at 274.9 °F, treating the live oil with 150 ppm of F-SiO_2 nanoparticles leads to over 600 psi delay of asphaltene onset pressure; however, in the presence of the same amount of Fe_2O_3 nanoparticles, the oil remains more stable and no asphaltenes precipitation is detected. Therefore, compared to the F-SiO_2, the Fe_2O_3 nanoparticles better control the asphaltene precipitation and aggregation. This may arise from the higher number and stronger interactions of the acidic/basic functional groups of the asphaltenes with the surface sites of the Fe_2O_3 nanoparticles. TEM images show that the size of irregular tangled asphaltene structures is decreased from 110 to 150 nm to 40−80 nm due to the addition of the nanoparticles to the live oil. Furthermore, the average interlayer spacing of the aromatic sheets of the asphaltene in aggregates is increased from 0.385 nm in blank live oil to 0.470 and 0.442 nm in the live oil treated with Fe_2O_3 and F-SiO_2, respectively. The consistency of different experimental results in this work provides invaluable insight for oil field applications of nanoparticles as a practical method to control the damages induced by asphaltene precipitation.

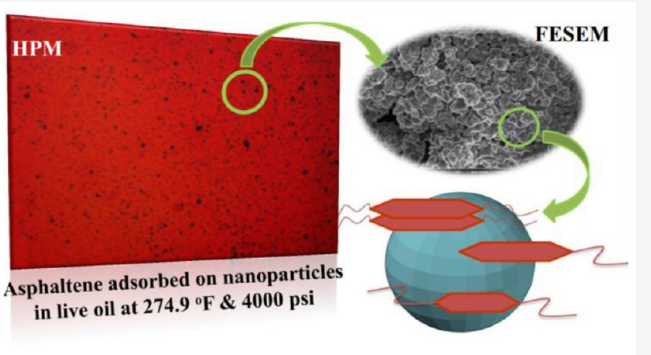

1. INTRODUCTION AND MOTIVATION

Nanoparticles, as an emerging tool, have gained considerable attention for their applications and solutions to the problems and challenges in different industries. By a quick literature survey, a growing trend in implementation of nanoparticles in the petroleum industry is obvious over the past decade. Nanoparticles are materials with particle diameters ranging in size from 1 to 100 nm, with large surface areas and high volume concentrations.[1] From these dimensional effects, nanoparticles possess unique mechanical, chemical, thermal, and magnetic properties. Therefore, they have a superior performance over conventional micro/macromaterials which offer prospective applications in oil and gas fields.[2] Nanoparticles/nanofluids have been applied to resolve issues in different sections of the petroleum industry such as drilling fluid enhancement,[3−5] gas hydrate production,[6,7] and enhanced oil recovery (EOR).[8−14]

During the past decade, nanoparticles have been suggested by many researchers as an alternative solution for traditional treatment techniques of asphaltene precipitation.[15−20] The precipitation and deposition of asphaltene from crude oil, as a major concern during oil production, have been well documented in the published literatures.[21,22] Asphaltenes constitute a high molecular weight fraction of crude oils which are insoluble in saturated hydrocarbons (e.g., *n*-pentane or *n*-heptane) and soluble in aromatic solvents (e.g., toluene or benzene).[23] Asphaltenes can be extremely problematic because of forming dense aggregates and deposits in reservoir porous media, wellbores, transportation pipelines, and processing facilities. Thus, they result in severe operational issues such as

Received: January 8, 2021
Revised: March 4, 2021
Published: March 16, 2021

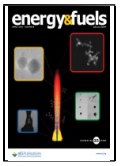

https://dx.doi.org/10.1021/acs.energyfuels.1c00060
Energy Fuels 2021, 35, 5908−5924

wettability alteration of reservoir rock, permeability reduction in near-wellbore regions, plugging tubulars and flowlines, clogging of production separators, reduction of well inflow performance, and increasing operating costs.[23,24]

The asphaltene precipitation in the presence of SiO_2, TiO_2, and ZrO_2 nanoparticles dispersed in paraffin at different pH conditions have been investigated.[16] Results showed that these nanoparticles may play the role of dispersant in strongly acidic conditions. It has been shown that NiO nanoparticles have a high affinity toward asphaltene adsorption in toluene model solutions.[25] Kazemzadeh et al. studied the effects of NiO nanoparticles on oil recovery and the mechanism of adsorption of asphaltenes in a synthetic oil solution.[18] Their results showed that increasing the asphaltene precipitant (n-C_7) content improves asphaltene adsorption on the surfaces of nanoparticles. Taborda et al. synthesized pure SiO_2, acidified silica (SiO_2A), and Al_2O_3 nanoparticles by the sol−gel method to study their effects on asphaltene precipitation in a model oil solution.[26] They found that evaluated nanoparticles were able to reduce the mean size of asphaltene aggregates in order of effectiveness: $SiO_2A < SiO_2 < Al_2O_3$. Shojaati et al. evaluated the inhibitory behavior of metal oxides nanoparticles, Fe_3O_4, NiO, and Al_2O_3, for postponement of the onset of asphaltene precipitation in a synthetic oil sample.[19] They concluded that used nanoparticles were effective on suppressing the onset point and reducing the amount of precipitated asphaltenes. López et al. investigated the effects of Cardanol/SiO_2 nanocomposites on formation damage by asphaltene precipitation in an asphaltene model solution.[27] They stated that adsorption of n-C_7 asphaltenes onto the surfaces of the Cardanol/SiO_2 nanocomposites decreased the amount of asphaltenes in the bulk solution and lessened the aggregation process.

A detailed literature survey shows that, to date, nearly all published works regarding the effects of nanoparticles on asphaltene precipitation have been carried out at ambient pressure and temperature with model oils containing synthetic asphaltenes extracted by addition of the saturated hydrocarbon (e.g., n-C_5 or n-C_7). Results and conclusions drawn from the synthetic asphaltene studies at laboratory conditions may not necessarily apply for asphaltenes precipitated in live oils at high pressure−high temperature (HPHT) conditions.[28] The only reported research with real crude oil is the work performed by Ahmadi and Aminshahidy.[29] They studied the effect of CaO and SiO_2 nanoparticles on the asphaltene precipitation envelope (APE) in the presence of miscible CO_2 gas. The authors prepared the oil sample by recombining the separator gas and crude oil in a PVT cell. They found that CaO and SiO_2 nanoparticles decreased the amount of precipitated asphaltenes in the presence of CO_2 gas, but CaO had better applications for reducing asphaltene precipitation.[29] It should be emphasized that a recombined oil sample may not be well restored to the initial conditions of the reservoir oil, mostly due to the irreversibility of the asphaltene precipitation.[30,31] Perfect operational decision-making scenarios to resolve asphaltene-related issues require precise experimental results. The first and main step for studying asphaltene-related subjects is to use a representative oil sample. The conventional sampler does not maintain fluid pressure above the threshold pressure of asphaltene precipitation while the sample is being retrieved to the surface;[32,33] thus, representative sampling is a prerequisite for asphaltene characterizations and studies. The collection of a nonrepresentative reservoir fluid sample may carry a nonrepresentative asphaltene amount because of the irreversible nature of asphaltene precipitation.[30,31] The most reliable reservoir sampler for studying asphaltene behavior is proposed to be a single-phase reservoir sampler (SRS) or one-phase sampler (OPS).[33−35] In addition, in the face of the extensive studies executed on the effect of iron oxide and silica-based nanoparticles on asphaltene precipitation, the feasible use of these types of nanoparticles at real pressure and temperature conditions has been grossly missing in the literature.

To address the above-mentioned challenges, in this work, two different nanoparticles, Fe_2O_3 and functionalized SiO_2 (F-SiO_2), were synthesized to evaluate and compare their effects on asphaltene precipitation and aggregation in a light live oil at HPHT conditions. To get a representative fluid sample for conducting precise experiments, the sampling was performed by OPS technology. Synthesized nanoparticles were characterized by X-ray powder diffraction (XRD), Fourier transform infrared (FTIR), field-emission scanning electron microscopy (FESEM), and Brunauer−Emmett−Teller (BET) techniques. Three sets of HPHT experiments were designed and performed by a solid detection system (SDS), high pressure microscopy (HPM), and HPHT filtration to evaluate the inhibitory and dispersion capacity of the synthesized nanoparticles toward asphaltene formation. To analyze the mechanisms of asphaltene−nanoparticle interactions, after conducting the HPHT experiments, the asphaltenes in blank live oil and the asphaltenes in live oil treated with nanoparticles were extracted and analyzed by FTIR, FESEM, transmission electron microscopy (TEM), and thermal gravimetric analysis (TGA). Finally, the industrial applications of the results obtained are discussed for different sections of the oil industry. To the best of our knowledge, this is the first study in which the potentials of nanoparticles for controlling the formation and growth of asphaltenes in live oil at HPHT conditions are investigated.

2. MATERIALS AND METHODOLOGY

2.1. Synthesis of Nanoparticles. Pure iron oxide Fe_2O_3 nanostructures were synthesized via a simple chemical precipitation method. In this procedure, first, to obtain a 0.05 M concentration solution, aqueous solution was prepared by dissolving an amount of iron(III) chloride hexa-hydrate ($FeCl_3$, $6H_2O$) in 100 cc of deoxygenated distilled water by magnetic stirring for 40 min at 80 °C. Then, a 50 cc aqueous solution of 2 M NH_4OH was used as the precipitating agent. NH_4OH as a base solution was added steadily dropwise to maintain a pH value of 11. The thus-obtained solution was heated to the temperature of 80 °C and stirred for about 3 h. The resultant precipitations were centrifuged at 5000 rpm for 10 min; then, the precipitates were washed with deionized water and ethanol several times and finally dried at 80 °C overnight. Then, the dried precipitates were calcined at 700 °C in static air for 3 h.

Sodium silicate with 25.5−28.5 wt % SiO_2 and 7.5−8.5 wt % Na_2O was used as the starting material for the synthesis of silica nanoparticles. At first, a water glass was diluted with different amounts of deionized water. Then, sodium ions were removed from the water glass using Amberlite−cation exchange resin (pH 2.3), and silicic acid with a concentration of 2 and 1 wt % of SiO_2 at pH 2.5−3.5 were obtained. Then, three alkaline sodium silicate solutions were prepared through diluting a water glass with deionized water for the preparation of solutions containing 1−3 wt % of SiO_2. These three alkaline sodium silicate solutions were heated at 84−86 °C, and titration was performed with similar volumes of silicic acids with different concentrations at a constant rate of 0.85 mL/min. Finally, the product was dried at 180 °C. For surface modification of silica

https://dx.doi.org/10.1021/acs.energyfuels.1c00060
Energy Fuels 2021, 35, 5908−5924

nanoparticles, amino-silane compounds were hydrolyzed and reacted with the silanol groups of silica particles. The reaction was performed at a temperature of 50 °C. After the reaction, the silica powders were filtrated and dried at 105 °C for about 1 h.

The crystal structures of the synthesized nanoparticles have been determined by XRD, with a PANalytical X'Pert PRO diffractometer, with a Cu Kα generator (60 kV, 40 mA, λ = 1.54060 Å) in the 2θ range from 5° to 140°. The textural properties of the nanoparticles have been analyzed by nitrogen adsorption−desorption at −196 °C with a porosimeter apparatus (ASAP-2010 Micromeritics, USA). The samples were degassed at 350 °C and 1.33−0.67 kPa prior to the N_2 adsorption experiments. Surface areas were calculated using the standard BET model. The pore size distribution (PSD) of the synthesized nanoparticles was estimated from the adsorption isotherms with the Barrett, Joyner, and Halenda (BJH) algorithm (built-in software from Micromeritics ASAP-2010). FESEM images were taken with a FEI Nova NanoSEM-450 to investigate the morphology and particle size of the synthesized nanoparticles. A PerkinElmer FTIR (version 10.4.2) spectrometer was utilized to characterize the surface functional groups of pure nanoparticles and nanoparticles with adsorbed asphaltenes. In FTIR analysis, the range of the scanning wavenumber was set to 4000−400 cm^{-1}.

2.2. Characteristics of Oil Sample. A light live oil was collected from an Iranian oil field using OPS technology with a LEUTERT one-phase sampler to have a representative oil sample. OPS sampling permits the reservoir fluid pressure to be maintained at or higher than the reservoir pressure during transfer and retrieval of the sample. The selected oil sample is from an oil field where severe operational issues induced by deposition of solid asphaltenic materials have been experienced and recorded. Table 1 shows the general properties of the oil sample and the results of saturates−aromatics−resins−asphaltenes (SARA) analysis. SARA analysis has been performed based on ASTM D2007-91, which is based on clay-gel adsorption chromatography.[36]

Table 1. Properties and Specifications of Oil Sample

specifications	unit	value	uncertainty
H_2S	mol %	0.24	$\pm5 \times 10^{-3}$
N_2	mol %	0.08	$\pm5 \times 10^{-3}$
CO_2	mol %	2.30	$\pm5 \times 10^{-3}$
C_1	mol %	48.72	$\pm5 \times 10^{-3}$
C_2	mol %	8.76	$\pm5 \times 10^{-3}$
C_3	mol %	5.02	$\pm5 \times 10^{-3}$
i-C_4	mol %	1.03	$\pm5 \times 10^{-3}$
n-C_4	mol %	2.92	$\pm5 \times 10^{-3}$
i-C_5	mol %	1.25	$\pm5 \times 10^{-3}$
n-C_5	mol %	1.31	$\pm5 \times 10^{-3}$
C_6	mol %	4.78	$\pm5 \times 10^{-3}$
C_7	mol %	3.48	$\pm5 \times 10^{-3}$
C_8	mol %	2.47	$\pm5 \times 10^{-3}$
C_9	mol %	3.41	$\pm5 \times 10^{-3}$
C_{10}	mol %	2.70	$\pm5 \times 10^{-3}$
C_{11}	mol %	2.92	$\pm5 \times 10^{-3}$
C_{12+}	mol %	8.61	$\pm5 \times 10^{-3}$
solution gas oil ratio	SCF/STB	1474.5	$\pm6 \times 10^{-2}$
reservoir temperature (T_R)	°F	274.9	$\pm5 \times 10^{-1}$
reservoir pressure (P_R)	psia	8700	±10
bubble point pressure (P_b)	psia	3837	±7
gravity of dead oil	°API	34.5	$\pm2 \times 10^{-1}$
molecular weight of reservoir oil	g/mol	81	$\pm6 \times 10^{-1}$
molecular weight of flash-residual oil	g/mol	204	$\pm6 \times 10^{-1}$
saturates	wt %	72.7	$\pm5 \times 10^{-4}$
aromatics	wt %	20.0	$\pm5 \times 10^{-4}$
resins	wt %	6.0	$\pm5 \times 10^{-4}$
asphaltenes	wt %	1.3	$\pm5 \times 10^{-4}$
colloidal instability index (CII)	−	2.85	−

Typically, before performing the expensive and time-consuming HPHT experiments, any reservoir fluid is screened to predict the risk of asphaltene precipitation. The most widely used screening criteria are the colloidal instability index (CII) and De Boer plot.[37,38] CII expresses as the ratio of the sum of asphaltenes and saturates fractions of crude oil to the sum of aromatics and resins.[37] The De Boer method is a graphical plot based on the solubility concept for prediction of the thermodynamic conditions for occurrence of asphaltene precipitation/deposition.[39] In the De Boer method, the difference in reservoir pressure and bubble point pressure is plotted versus reservoir fluid density. For the studied oil sample here, the CII value (reported in Table 1) is 2.85, which confirms the instability of the asphaltene in the oil sample. On the basis of the De Boer method, the oil sample is located in unstable regions; thus, it is recognized as unstable or problematic oil with the possibility of solid phase problems during the production life of the reservoir. The structure and combustion trend of the precipitated asphaltenes were analyzed by TEM (Philips-EM208S operating at 100 kV) and TGA (NETZSCH TG 209), respectively.

2.3. Procedures of HPHT Experiments. To evaluate the effect of the synthesized nanoparticles on inhibition and dispersion of asphaltene precipitation, a SDS setup (manufactured by the DBR-Schlumberger, Edmonton, Canada) equipped with NIR transmittance detector and a HPM was utilized. The maximum working pressure and temperature for the SDS and HPM systems are 15,000 psi and 350 °F. In addition, a HPHT filtration apparatus was used to measure the amount of the precipitated asphaltenes at different conditions of pressure and temperature without and with nanoparticles. The HPHT filtration apparatus gives proper results at a range of pressure and temperature up to 10,000 psi and 350 °F. The photos of the SDS-HPM assembly and HPHT filtration apparatus are shown in Figures 1 and 2, respectively.

2.3.1. Procedure of SDS Experiments. SDS experiments were performed in a HPHT laser cell, which measures the NIR turbidity as a function of pressure at constant temperature. In addition, using SDS, the bubble point of reservoir oil can be determined by a classical P−V curve as well as a visual observation that can be used as a checking procedure for the PVT test. The live oil sample is transferred from the sample cylinder into the SDS cell at an initial pressure (9000 psi) and constant temperature (274.9 °F). The sample is equilibrated for about 24 h before isothermal depressurization of the fluid at predefined rates of 15−20 psi/min from the initial reservoir pressure to the bubble point pressure. At the bubble point, the light transmittance power (LTP) through the fluid in the PVT cell is approximately zero due to the evolution of gas bubbles. Any sudden change before the bubble point pressure in the LTP is an indication of the appearance of solids in the reservoir fluid, which is shown in the graphical display. The detailed procedure of the SDS experiment is described by Mohammadi et al.[40]

2.3.2. Procedure of HPM Experiments. The HPM permits to one monitor the onset and the growth of asphaltenes as a function of pressure, temperature, and composition and hence to describe the morphological behavior of the asphaltene aggregates. It is also utilized to study the effects of different types of chemicals on asphaltene precipitation. It consists of a cell with two sapphire windows, a long focal length camera of high resolution, and a light source. The cell thickness is 0.3 mm, and the diameter of the sapphire is 9.2 mm. However, the cell thickness can be adjusted to a desirable value. The cell temperature is controlled by a circulation bath, manufactured by the Huber-GmbH Company, whereas the fluid pressure inside the cell is maintained using a positive displacement pump. In this work, an HPM model Leica Z16-APO with total magnification of approximately 1000X was used to investigate the effect of Fe_2O_3 and F-SiO_2 nanoparticles on formation and growth of asphaltene particles. The cell contents were observed visually, and the images were recorded by the HPM video camera during the course of the experiment. High-resolution photographs of the sample were taken at specified pressure steps to monitor the aggregation process in blank live oil and treated live oil with nanoparticles. The taken images were processed by the Java-based *ImageJ* package, version 1.44, developed at the National

https://dx.doi.org/10.1021/acs.energyfuels.1c00060
Energy Fuels 2021, 35, 5908−5924

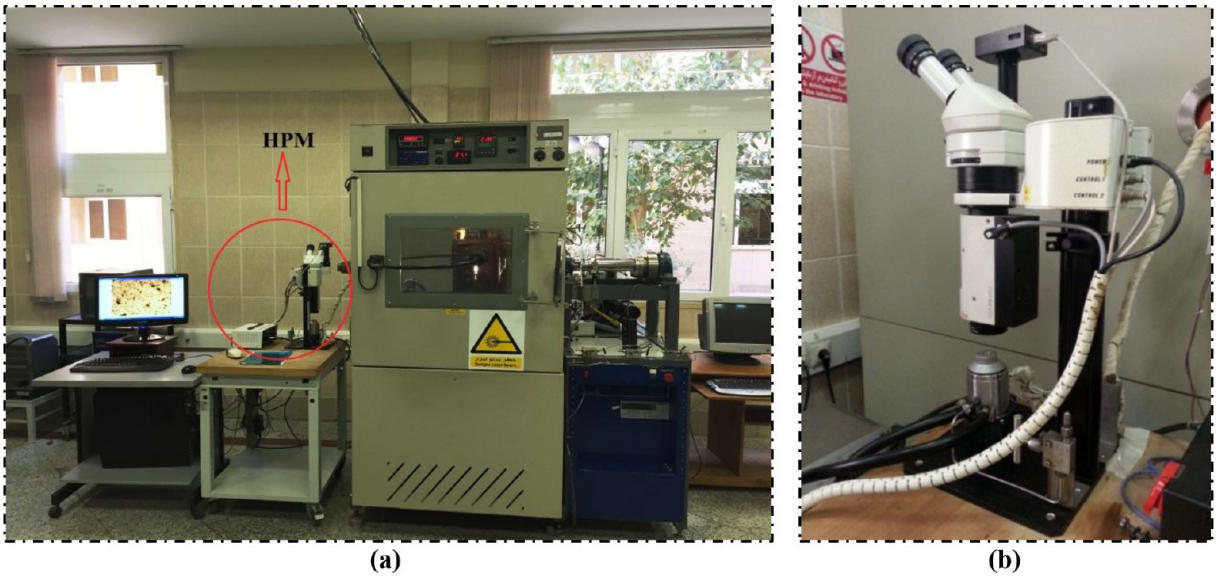

Figure 1. (a) Picture showing the SDS equipped with NIR transmittance and HPM. (b) Close-up view of HPM.

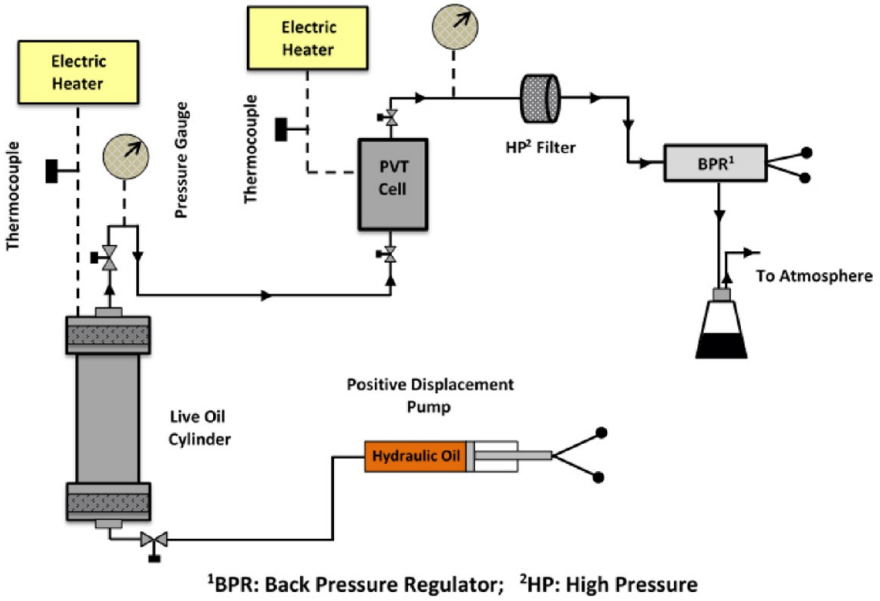

Figure 2. Schematic diagram of HPHT filtration setup. Reproduced from ref 40. Copyright 2015, American Chemical Society.

Institutes of Health.[41] Detailed descriptions of the HPM procedure can be found elsewhere.[42,43]

2.3.3. Procedure of HPHT Filtration Experiments. HPHT filtration tests were conducted with a 0.20 μm cellulose nitrate filter to evaluate the effect of the nanoparticles on the amount of precipitated asphaltene versus pressure during the isothermal depressurization process. To start the experiment, about 120−150 cc of blank live oil was transferred isobarically and isothermally into the PVT cell. For each experiment, the PVT cell was stabilized at the initial pressure and temperature of the test for 72 h. After stabilization of the fluid inside the PVT cell, the pressure was lowered at predefined pressure steps. At each pressure step, the cell content was homogenized for 24 h. Then, the fluid was displaced through the filter, and about 10 cc of well-mixed fluid sample was expelled from the PVT cell at the pressure and temperature of the experiment to flash to the atmospheric condition. Then, the asphaltene content was measured by an IP-143 standard test (ASTM D3279-90) to determine the amount of precipitated asphaltenes.[44] During the filtration process, it is essential that the oil sample remains monophasic at each pressure step above the bubble point pressure as it passes through the filter manifold. Thus, high pressure helium gas is used on the backside of the filter to keep a back-pressure on the downstream end of the filter. This helps to conduct the HPHT filtration process at almost constant pressure conditions. To better understand the experimental protocol in this work, procedures are schematically described in Figure 3.

2.4. Treating Live Oil Sample with Nanoparticles. For the sake of comparison, the SDS, HPM, and HPHT filtration experiments were conducted in both the absence and presence of the nanoparticles dispersed in the live oil. To disperse the nanoparticles in live oil (named as treated oil), a certain amount of nanoparticles was added to an empty high pressure cylinder at ambient conditions. Then, a known amount of the live oil sample was injected into the high pressure cylinder at constant pressure such that the nanoparticle dosage was known in the thus-obtained HPHT sample. Then, the cylinder content was well shaken and homogenized at an initial pressure. For the SDS, HPM, and HPHT filtration tests in the presence of the nanoparticles, a specified amount of the treated oil was utilized to conduct the subsequent investigations.

https://dx.doi.org/10.1021/acs.energyfuels.1c00060
Energy Fuels 2021, 35, 5908−5924

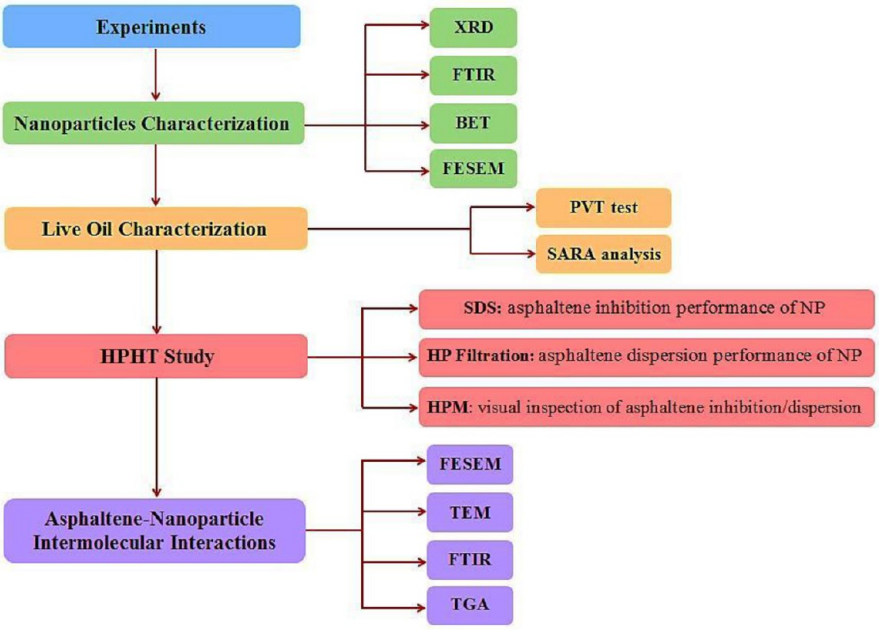

Figure 3. Schematic illustration of experimental procedures.

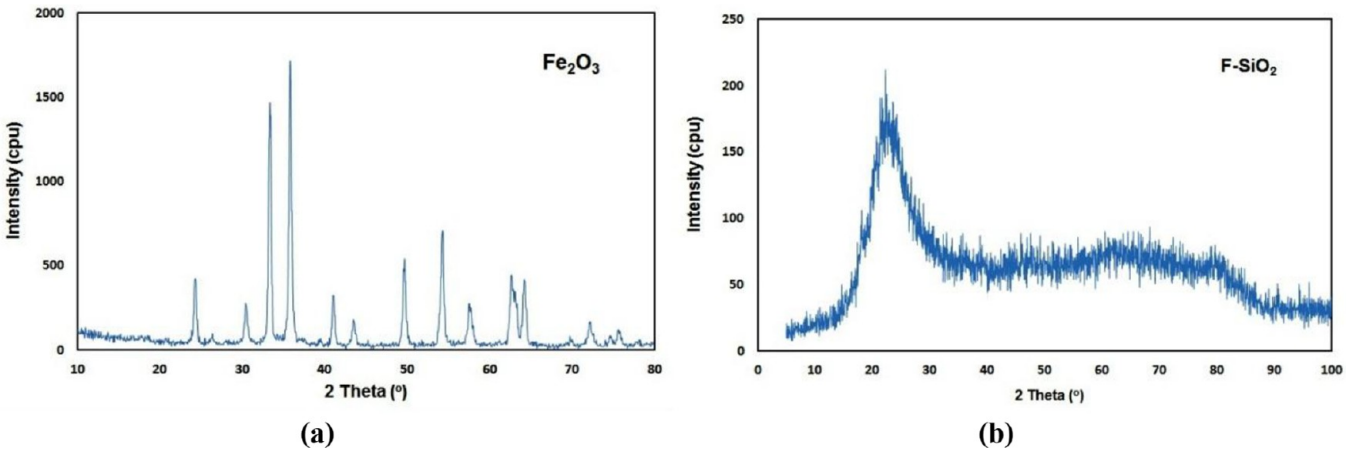

Figure 4. XRD patterns of synthesized nanoparticles: (a) Fe_2O_3 and (b) F-SiO_2.

As HPHT experiments are costly and time consuming, an optimum nanoparticle concentration should be selected for the HPHT conditions. So, the efficiencies of both Fe_2O_3 and F-SiO_2 nanoparticles for inhibition and dispersion of asphaltene were evaluated by viscometry experiments at dosages of 75, 150, 200, 300, and 500 ppm. On the basis of the obtained results, for both nanoparticles, the dosage of 150 ppm was chosen as the optimum loading since a plateau was observed in the efficiency curve. This nanoparticle dosage is in the range of reported concentrations by other researchers.[45,46] The procedure for determination of optimum dosage of the nanoparticles for HPHT experiments is presented in the Supporting Information.

3. RESULTS AND DISCUSSION

3.1. Characterization of Synthesized Nanoparticles. The XRD patterns of the synthesized Fe_2O_3 and F-SiO_2 nanoparticles are illustrated in Figure 4. In Figure 4a, all detected peaks are indexed to the rhombohedral crystal structure of pure Fe_2O_3. The peaks appearing at the 2θ range of 24.25°, 33.35°, 35.80°, 41.10°, 49.70°, 54.30°, and 57.50° can be attributed to the (012), (104), (110), (113), (024), (116), and (018) crystalline structures of pure Fe_2O_3 (JCPDS no. 06-0696), respectively. As is observed in Figure 4b, the presence of a wide peak at 22.28° confirms the good development of the amorphous F-SiO_2 structure during the synthesis process.

Nitrogen adsorption−desorption isotherms for the synthesized Fe_2O_3 and F-SiO_2 nanoparticles at the liquid nitrogen temperature are shown in Figure 5a and b. According to the IUPAC classification, the isotherm trend displays a type-V curve and a sensible hysteresis loop in the range of $P/P_o > 0.8$ for Fe_2O_3, and $P/P_o > 0.7$ for F-SiO_2. This curve type for both Fe_2O_3 and F-SiO_2 nanoparticles is a clear indication of mesoporous materials consisting of approximately uniform sphere particles.[47] The pore size distribution of the synthesized nanoparticles by BJH theory are shown in Figure 5c and d. The main pore size fits the mesoporous scale, 2−50 nm, which is considered as an important class of nanoparticle materials for asphaltene adsorption due to the sizes of the asphaltene molecular structures. The textural and surface properties of synthesized nanoparticles by N_2 adsorption experiments are given in Table 2. The specific surface area by the BET model

https://dx.doi.org/10.1021/acs.energyfuels.1c00060
Energy Fuels 2021, 35, 5908−5924

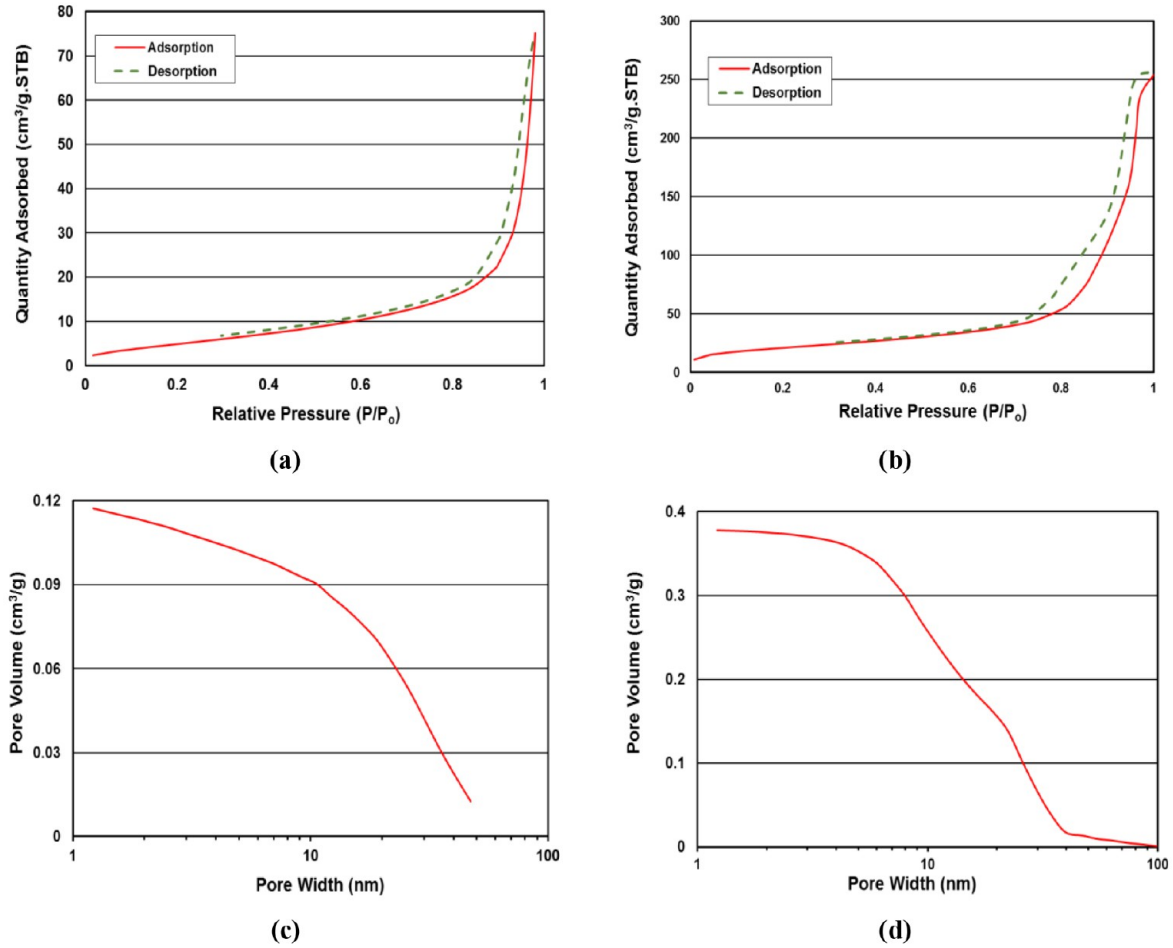

Figure 5. (a, b) Nitrogen adsorption−desorption isotherms of Fe_2O_3 and F-SiO_2 nanoparticles, respectively. (c, d) Pore size distribution of Fe_2O_3 and F-SiO_2 nanoparticles, respectively (BJH measurements).

Table 2. Textural and Surface Properties of Synthesized Nanoparticles

specification	unit	Fe_2O_3	F-SiO_2
BET specific surface area, A_{BET}	(m^2/g)	20.197	73.705
average particle size, d_{ave}	(nm)	51.75	30.72
average pore diameter, d_{BET}	(nm)	23.04	20.78
average pore diameter, d_{BJH}	(nm)	18.67	20.09
total pore volume of pores	(cm^3/g)	0.1164	0.3829
BJH cumulative pore volume	(cm^3/g)	0.1173	0.3777

for Fe_2O_3 and F-SiO_2 nanoparticles is obtained to be 20.197 and 73.705 m^2/g, respectively, which is high enough for asphaltene adsorption. The average diameters of the nanoparticles by the BET model (d_{BET}) and BJH method (d_{BJH}) have been calculated from the 4V/A formula[48] as given in Table 2. In this formula, V and A are the pore volume and specific surface area, respectively. Supposing a spherical shape for the nanoparticles as demonstrated from Figure 5a and b, the average sizes of the particles can be estimated by $d_{ave} = 6000/(\rho \times A_{BET})$,[49] where ρ is the density of the nanoparticles in g/cm^3 and A_{BET} is the specific surface area of the nanoparticles in m^2/g. The average sizes of the nanoparticles by BET are in agreement with the results of FESEM analysis. The FESEM and FTIR analyses of pure nanoparticles along with adsorbed asphaltenes onto the surface of nanoparticles are discussed in detail in Section 3.5.

3.2. Results of SDS Experiments. The traces of SDS during the isothermal depressurization process at a temperature of 274.9 °F for the blank live oil and the treated live oil with 150 ppm Fe_2O_3 and F-SiO_2 nanoparticles are shown in Figure 6. All these experiments were started from the initial pressure of 9000 psi down to near of the bubble point pressure where the light transmittance power through the fluid in the PVT cell suddenly drops to about zero due to the instantaneous scattering of the laser light caused by the evolution of gas bubbles. As shown in Figure 6, the asphaltene onset pressure (AOP) of the original live oil at 274.9 °F is detected at the pressure of 7383 psia in which the increasing trend of the LTP signal starts to decrease gradually (curve in red on the graph). During the isothermal depressurization of the oil sample, the LTP signal increases linearly because of a decrease in fluid density by a pressure decrement until the formation of detectable asphaltenic aggregates, where the LTP starts to drop because of growth of the asphaltene aggregates (i.e., asphaltene aggregation process). This inflection point of the LTP on the graph is recognized as AOP. It should be noted that based on the supplied laser power the minimum detectable asphaltene size by SDS is approximately 1−2 μm, which corresponds to detected AOP. The green and blue curves in Figure 6 depict the traces of SDS in the presence of Fe_2O_3 and F-SiO_2 nanoparticles, respectively. The overall trend of the depressurization path is the same as for the case of blank

https://dx.doi.org/10.1021/acs.energyfuels.1c00060
Energy Fuels 2021, 35, 5908−5924

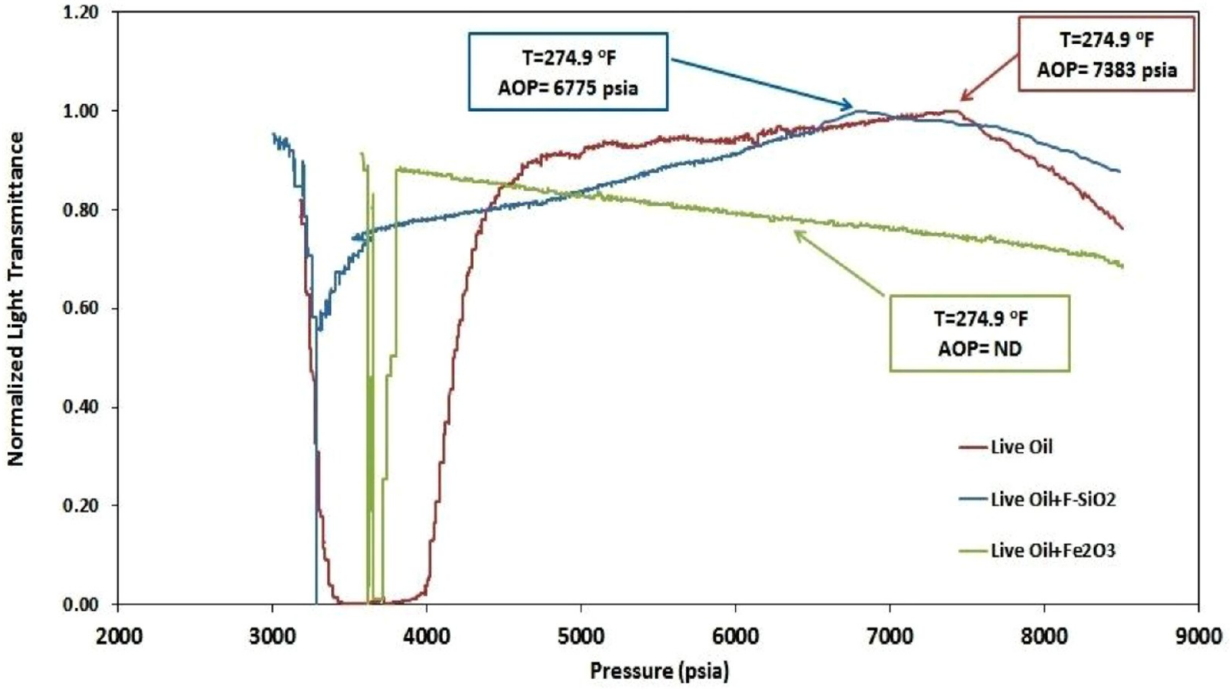

Figure 6. SDS isothermal depressurization at 274.9 °F for blank live oil and treated live oil with 150 ppm Fe_2O_3 and F-SiO_2 nanoparticles.

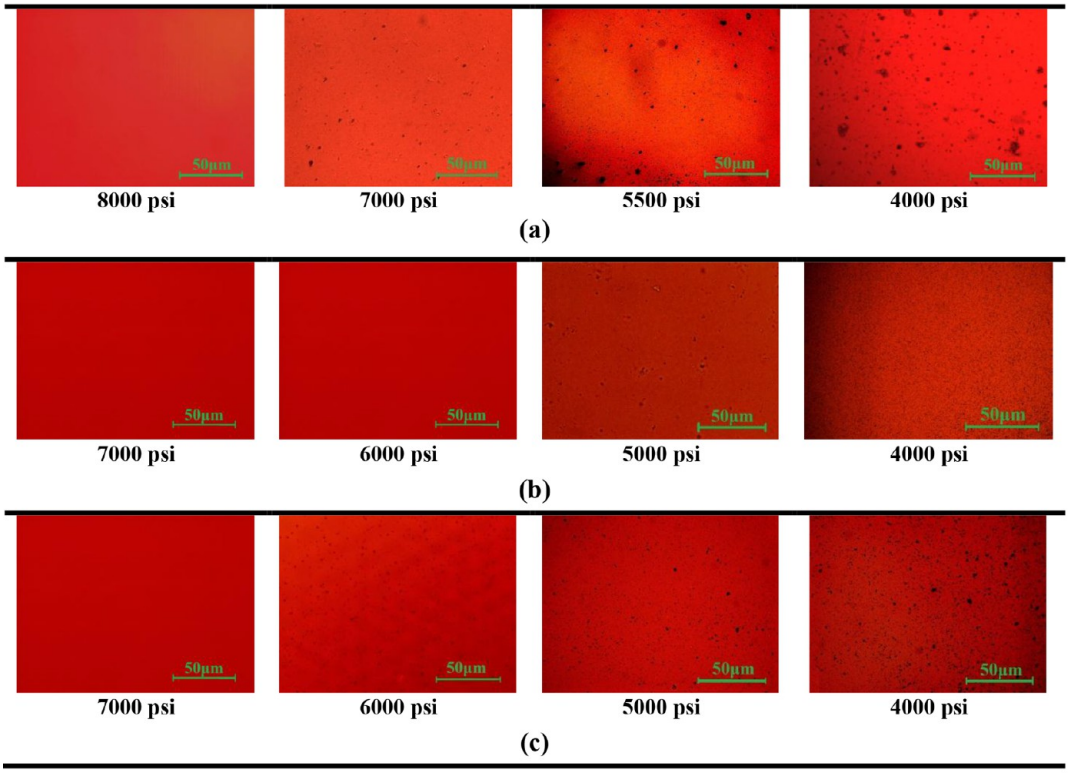

Figure 7. HPM visualization of asphaltene precipitation−aggregation behavior at 274.9 °F: (a) blank live oil, (b) treated live oil with 150 ppm Fe_2O_3, and (c) treated live oil with 150 ppm F-SiO_2; images were processed by *ImageJ*.

live oil. However, the AOP in the presence of 150 ppm of the F-SiO_2 is detected at 6775 psia, a shift of about 608 psi to lower pressures, indicating the tardiness in the asphaltene precipitation by the F-SiO_2 nanoparticles. For the case of Fe_2O_3 nanoparticles, the LTP signal during isothermal depressurization increases progressively up to the pressures around 3900−4000 psia; then, an abrupt change in LTP is observed as a result of gas bubbles evolution (i.e., bubble point pressure). The detected bubble point pressure is nearly in line with the measured bubble point pressure from the constant composition expansion (CCE) experiment (3837 psia), reported in Table 1. However, by the addition of 150 ppm Fe_2O_3 into the live oil, within the accuracy range of the SDS, no asphaltene particle was detected down to near the bubble

https://dx.doi.org/10.1021/acs.energyfuels.1c00060
Energy Fuels 2021, 35, 5908−5924

point pressure. Therefore, this may infer that the oil remains stable in the presence of the Fe_2O_3 nanoparticles since no asphaltene precipitation is detected during the depressurization process at 274.9 °F.

It should be mentioned that the bubble point pressure of the blank live oil sample by the routine CCE-PVT experiment is 3837 psia, as reported in Table 1. In addition, SDS experiments for blank live oil and treated live oil with Fe_2O_3 and F-SiO_2 nanoparticles visually confirm the obtained bubble point pressure by CCE, which is depicted as abrupt changes in LTP through the fluid. In Figure 6, for blank live oil and treated live oil with F-SiO_2, asphaltene particles start to precipitate out at detected AOPs. Then, the precipitated particles go through self-association and growth at pressures lower than AOP to around bubble point pressure. At around the bubble point, the abrupt LTP decline is a result of both the evolution of gas bubbles and the presence of asphaltene aggregates. Therefore, the overlapping of the effects of the presence of gas pockets and asphaltene aggregates in the liquid may hinder the solid determination of the liquid bubble point pressure by SDS data (shown on graph in Figure 6). However, for all SDS experiments (i.e., blank and treated live oils), observations of the fluid inside the visual PVT cell in the SDS setup confirm that bubble point take places at 3837 psia. For live oil treated with Fe_2O_3 nanoparticles, as asphaltene does not precipitate out, the sudden changes observed in the LTP at around 3870 psia can be assigned to the presence of gas bubbles only.

3.3. Results of HPM Experiments. Asphaltene precipitation and the aggregation process in blank live oil and treated live oil with 150 ppm Fe_2O_3 and F-SiO_2 nanoparticles are visualized by HPM experiments at different pressure steps and a temperature of 274.9 °F. Microscopic images of the HPM experiments are shown in Figure 7. The average sizes of asphaltene aggregates versus pressure are given in Table 3. In addition, as an example case, the size distributions of the aggregates at 4000 psi are shown in Figure 8. HPM detects asphaltene sizes higher than 0.50−0.60 μm. Thus, the onset pressure of asphaltene precipitation by HPM is somewhat higher than the onset pressure by the SDS technique for each oil sample.

Table 3. Average Size of Asphaltene Aggregates (d_{ave}) vs Pressure at 274.9 °F (HPM Experiments)[a]

pressure (psi)	d_{ave} in blank live oil (μm)	d_{ave} in treated live oil with Fe_2O_3 (μm)	d_{ave} in treated live oil with F-SiO_2 (μm)
7000	1.15	–	–
6000	2.34	–	1.10
5000	4.06	0.80	2.06
4000	8.07	1.38	4.14

[a]The uncertainty in the pressure measurement is ±7 psi. The uncertainty in the calculation of the average size is $\pm 2.5 \times 10^{-3}$ μm.

As depicted in Figure 7a, in blank live oil, in the range of a microscope resolution at 8000 psi, the sample is uniform, with no asphaltene particles present. At the 7000 psi pressure step, some distinct asphaltene particles are observed. These particles continue growing from the nanoscale until they reach the micrometer scale and can subsequently be seen under a microscope. With a decrease in pressure from 7000 to 5500 psi, the number of detectable aggregates increases as the growth continued, and large aggregates are present in the sample. Further pressure reduction to 4000 psi results in severe intensification of aggregation of asphaltenes with an average particle size of about 8.07 μm. It is clear from Figures 7b and 8 that treating of live oil with Fe_2O_3 nanoparticles at 150 ppm leads to much slower aggregation of asphaltenes with a uniform size distribution at different pressure steps. It is observed that at a pressure of 4000 psi the average size of asphaltene aggregates is 1.38 μm, which is much smaller than the average size of aggregates in blank live oil. A comparison of the results obtained for the blank live oil with those obtained for the live oil treated with Fe_2O_3 indicates that Fe_2O_3 can serve as an excellent asphaltene inhibitor and dispersant for stabilizing asphaltene particles in oil with controlling the rate of asphaltene aggregation.

HPM images in Figure 7c demonstrate that in the presence of 150 ppm of the F-SiO_2 nanoparticles the formation and aggregation growth of asphaltenes by pressure reduction are controlled and suppressed when compared to the asphaltene aggregation process in the blank live oil. However, as given in Table 3, for F-SiO_2 nanoparticles, the asphaltene particle sizes are larger than in the case of Fe_2O_3 nanoparticles at corresponding similar pressure steps. It can be inferred from the data in Table 3 that the average sizes of asphaltene aggregates at different pressures are in decreasing order of (blank oil + Fe_2O_3) < (blank oil + F-SiO_2) < (blank oil). Better performance of Fe_2O_3 nanoparticles compared to F-SiO_2 nanoparticles in controlling the rate of asphaltene aggregation in studied live oil is ascribed to the high number and strong interactions of the surface sites of the Fe_2O_3 nanoparticles with the functional groups of mostly the unstable fraction of the asphaltenes. This leads to a diminished self-association tendency of the asphaltenes and thus the absence of enough and effective nucleation sites for growth and precipitation of asphaltene aggregates in the presence of the nanoparticles.[50,51] It is worth noting that the effective nucleation sites are expected to start to form by the self-association/aggregation of the most unstable fraction of the asphaltene in the live oil, followed by aggregation and growth of the nucleates through adsorption of lighter fractions of the asphaltenes. As well, the higher potential of Fe_2O_3 for control of asphaltene aggregation can be explained by the higher number and strength of the interactions of the iron oxide surface sites with the acidic and basic functional groups of the asphaltene particles.[17] In other words, Fe_2O_3 nanoparticles more quickly attract asphaltenes due to their higher adsorption affinity compared to the F-SiO_2 nanoparticles. Thus, stronger polar interactions are formed between asphaltenes and Fe_2O_3 nanoparticles, which are mainly acidic/basic. In addition, the higher capacity of iron oxide for asphaltene adsorption weakens some of the interactions between the asphaltene nanoaggregates in the bulk medium of the oil phase. Therefore, Fe_2O_3 nanoparticles more efficiently control the aggregation of asphaltenes in comparison to the F-SiO2 nanoparticles. It should be stated that the results of HPM experiments for slower aggregation of asphaltenes in the presence of synthesized nanoparticles support the obtained results by SDS experiments.

3.4. Results of HPHT Filtration Experiments. Isothermal HPHT filtration experiments were designed at specific pressure steps in a single-phase region to measure the amount of precipitated asphaltenes in blank live oil and treated live oil with the synthesized nanoparticles at the dosage of 150 ppm. The results of the HPHT filtration experiments are presented in Figure 9 and Table 4. As is inferred from the overall trend in

https://dx.doi.org/10.1021/acs.energyfuels.1c00060
Energy Fuels 2021, 35, 5908−5924

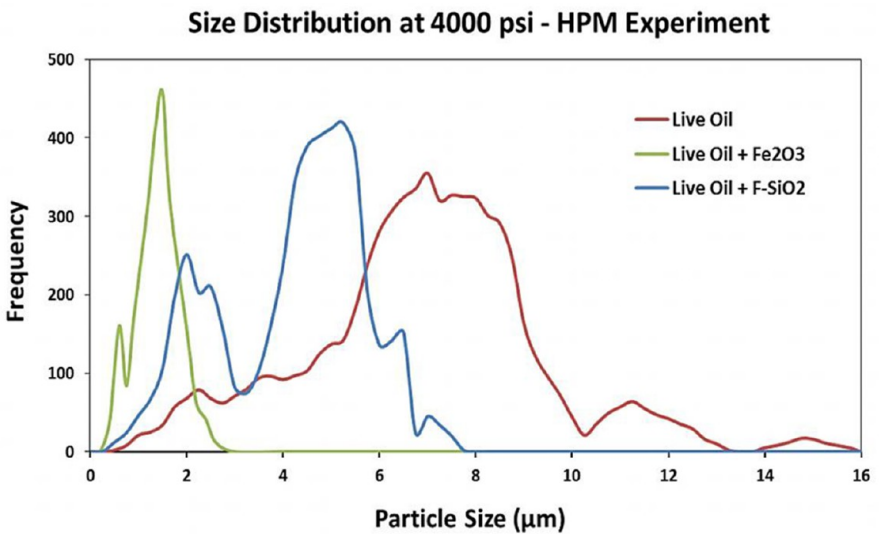

Figure 8. Size distribution of asphaltene particles for blank live oil and treated live oil with 150 ppm Fe_2O_3 and F-SiO_2 at 4000 psi and temperature of 274.9 °F (HPM experiments).

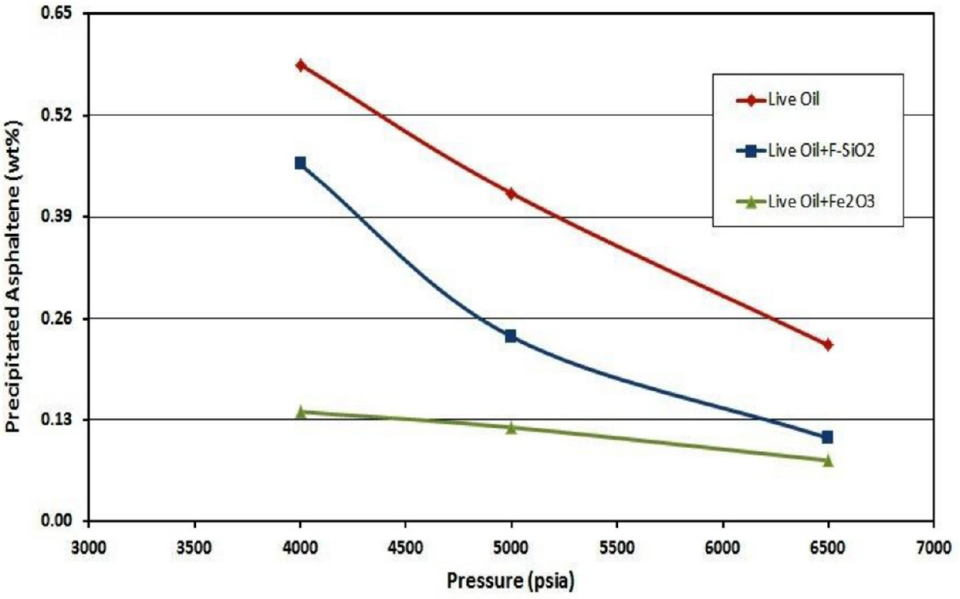

Figure 9. Amount of precipitated asphaltene by HPHT filtration during depressurization at 274.9 °F for blank live oil and treated live oil with 150 ppm Fe_2O_3 and F-SiO_2. The uncertainty in the measurement of the precipitated asphaltene weight percent is $\pm 1 \times 10^{-4}$ wt %.

Table 4. Amount of Precipitated Asphaltene by HPHT Filtration at 274.9 °F

pressure (psi)	precipitated asph in blank live oil (wt %)	precipitated asph in live oil with Fe_2O_3 at 150 ppm (wt %)	precipitated asph in live oil with F-SiO_2 at 150 ppm (wt%)
6500	0.226	0.078	0.107
5000	0.420	0.120	0.237
4000	0.586	0.141	0.458

[a]The uncertainty in the pressure measurement is ±7 psi. The uncertainty in the precipitated asphaltene weight percent is $\pm 2 \times 10^{-4}$.

Figure 9, the amount of asphaltene precipitation increases as pressure decreases down to the bubble point pressure for all performed experiments. The increase of precipitated asphaltene by pressure depletion for pressures higher than the bubble point pressure is explained by solubility theory. By pressure reduction at a single-phase state, the molar volume of light end paraffinic components of the oil, which act as asphaltene precipitants, increases relatively more than that of the heavy end components. Therefore, it causes s less volumetric-based aromatic state for oil and reduction of asphaltene solubility, which results in an increase in asphaltene precipitation.

The obtained results show that in the presence of the nanoparticles the amount of precipitated asphaltenes decreases in comparison to the blank live oil (Figure 9 and Table 4). However, the performance of iron oxide nanoparticles in the reduction of asphaltene precipitation is more pronounced than the synthesized functionalized silica-based nanoparticles. On the basis of the obtained HPHT filtration results, the addition of Fe_2O_3 nanoparticles into the light oil sample leads to precipitation of just 0.141 wt % of asphaltenes, larger than 0.20 μm in size, by pressure reduction from 6500 to 4000 psi. For the case of F-SiO_2, the asphaltene precipitate amount in the

https://dx.doi.org/10.1021/acs.energyfuels.1c00060
Energy Fuels 2021, 35, 5908−5924

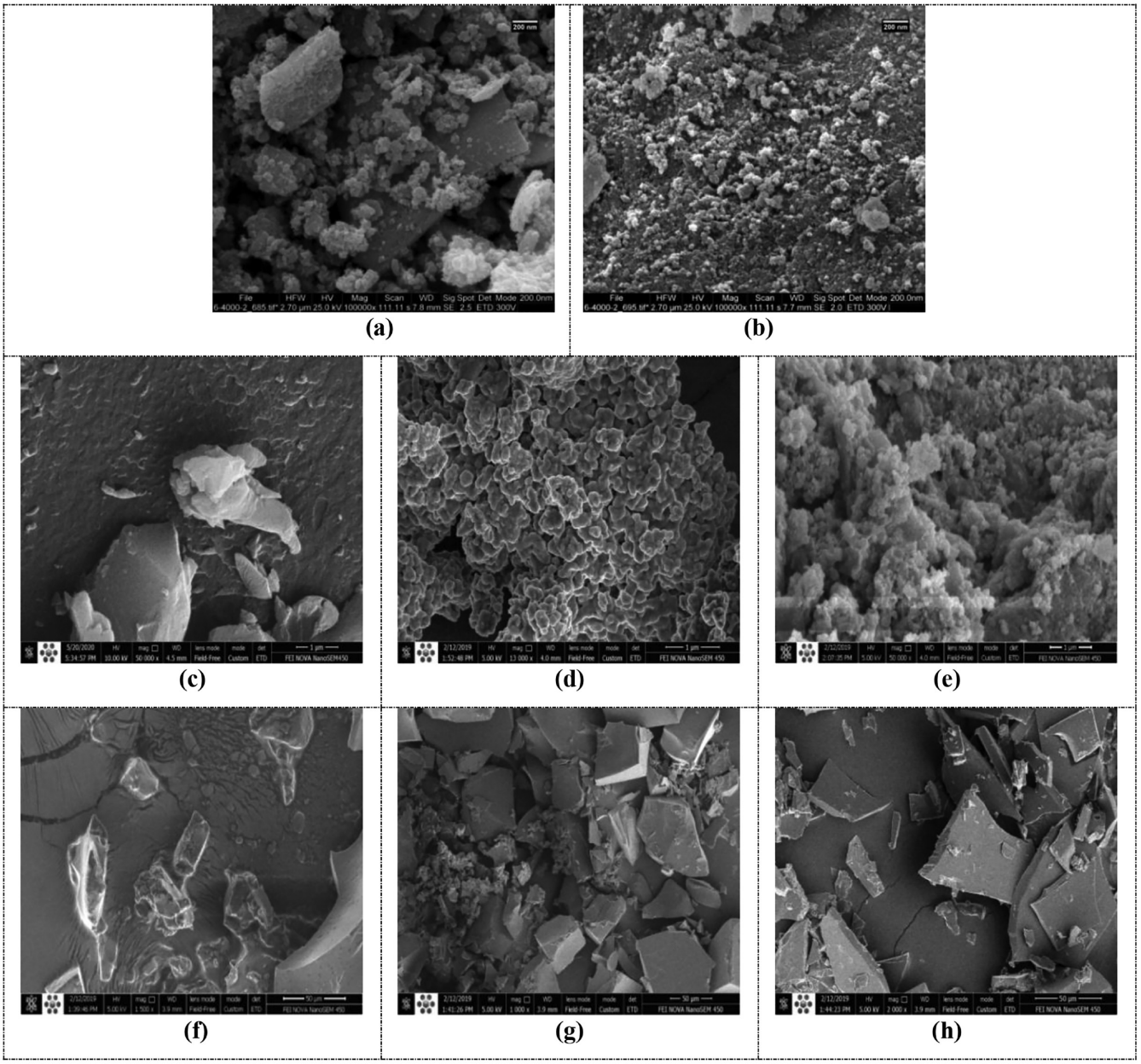

Figure 10. FESEM images of (a, b) pure Fe_2O_3 and F-SiO_2 at 200 nm scale, respectively, (c, d, e) pure and adsorbed asphaltenes onto Fe_2O_3 and F-SiO_2 at 1 μm scale, respectively, (f, g, h) asphaltene aggregates without and with Fe_2O_3 and F-SiO_2 at 50 μm scale, respectively; asphaltenes were extracted from live oil after HPHT filtration experiments.

pressure range from 5000 to 4000 psi increases sharply from 0.237 to 0.458 wt % in comparison to the precipitated asphaltenes by pressure reduction from 6500 to 5000 psi. It is depicted by a sharp change in slope of the blue curve in Figure 9 between 5000 and 4000 psi. However, Fe_2O_3 nanoparticles have caused more dispersion/suspension of asphaltene aggregates in comparison to the F-SiO_2 nanoparticles. As discussed in a previous section, it is attributed to the higher number of strong interactions of the asphaltenes with the Fe_2O_3 nanoparticles.

3.5. Intermolecular Interactions between Nanoparticles and Asphaltene. After performing HPHT filtration experiments, pure asphaltenes precipitated in blank live oil sample and adsorbed asphaltene onto the nanoparticles were extracted by the IP-143 method. Then, the asphaltene–nanoparticle interactions and asphaltene adsorption behavior onto the surface of nanoparticles were explored by FESEM, TEM, FTIR, and TGA. It should be clarified that chemical and physical properties of the extracted asphaltenes from the live oil are completely different from the asphaltenes precipitated in dead oil at standard laboratory conditions, called as synthetic asphaltene. Asphaltenes in live oil, which are stabilized by association of the resin fraction of the oil, are destabilized because of the reduction of the bulk oil dielectric constant during the depressurizing process,[28,52] while synthetic asphaltenes are formed by titration of the crude oil with normal alkane solvents (e.g., *n*-C_7). In synthetic asphaltenes formed at ambient conditions, destruction of asphaltene micelles occurs, and they are friable with no resinous materials. As in this work, the asphaltenes are extracted from the live oil

https://dx.doi.org/10.1021/acs.energyfuels.1c00060
Energy Fuels 2021, 35, 5908−5924

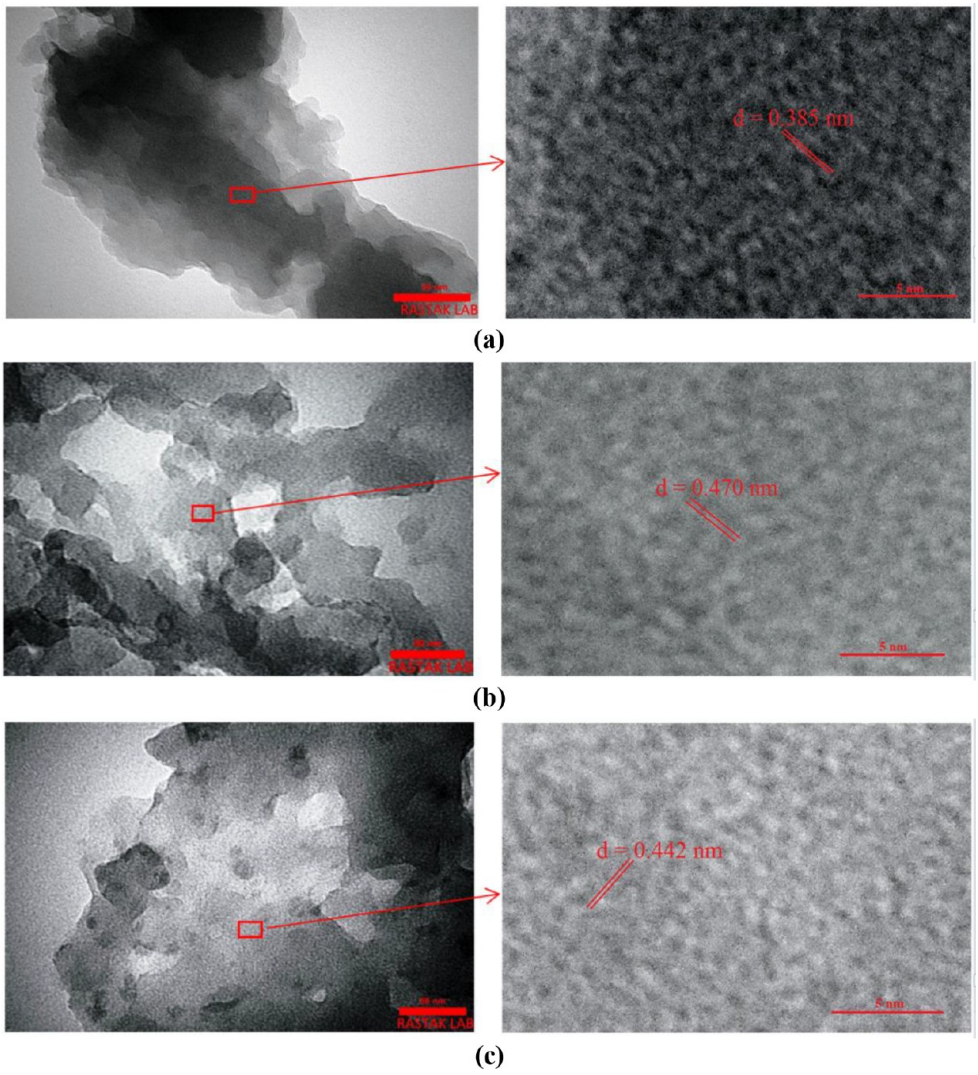

Figure 11. TEM images of (a) pure asphaltene and (b, c) Fe_2O_3 and F-SiO_2 nanoparticles after asphaltene adsorption, respectively. Darkness reduction of TEM images in (b) and (c) in comparison to (a) proves that addition of nanoparticles to the oil prevents severe asphaltene aggregation and formation of thick and dense asphaltene flocs.

samples during depressurization, and the asphaltene−nanoparticle interactions have occurred in a real oil medium at elevated pressures and temperatures. Thus, the behavior of asphaltene adsorption onto the surface of nanoparticles and subsequent asphaltene−nanoparticle interactions negligibly change during the extraction process. Accordingly, the obtained results reflect the asphaltene adsorption behavior at HPHT conditions.

3.5.1. FESEM Analysis. FESEM analyses have been performed on synthesized nanoparticles before and after adsorption of asphaltenes to study the surface morphologies of the samples (Figure 10). FESEM observations have shown that Fe_2O_3 nanoparticles are nearly rough elliptical in shape; the average size of the pure Fe_2O_3 is about 40−60 nm (Figures 10a). Surface morphology of the F-SiO_2 sample (Figure 10b) indicates uniformly sphere-like nanoparticles with sizes in the range of 25−40 nm. The average sizes of the synthesized nanoparticles by FESEM are in line with the results obtained from the BET measurements (Table 2).

The FESEM image in Figure 10c shows that the structure of pure asphaltene comprises both smooth and rough surfaces on which agglomerated particles are deposited. These agglomerates are most likely attributed to the presence of resinous materials or maltene fractions of oil that are normally attached to the structure of asphaltene as a support for their dispersion in bulk of oil.

In comparison to pure nanoparticles, for nanoparticles with adsorbed asphaltenes, the morphology of the surface forms an irregular shape with distinct boundaries, as observed in Figure 10d, e, g, and h. The irregular structure of nanoparticles is related to the adsorption of asphaltenes onto the surface of nanoparticles, which leads to weaker interactions of nanoparticles with neighboring undecorated particles. Also, the adsorbed asphaltenes onto the surface of nanoparticles are stabilized, and their affinities toward dispersed asphaltenes in the bulk medium of oil or those adsorbed onto the adjacent nanoparticles are abated. This adsorption phenomenon, in principle, assists with more stability and dispersion of asphaltenes and controls the growth process of the asphaltene aggregates sizes in the nanometer scale. Higher magnification of Figure 10f compared with Figure 10c has indicated that the surfaces of asphaltene aggregates became more fragmental and shattered with formation of deep grooves and cleavage fracture patterns. The formation of these patterns may be the result of

https://dx.doi.org/10.1021/acs.energyfuels.1c00060
Energy Fuels 2021, 35, 5908−5924

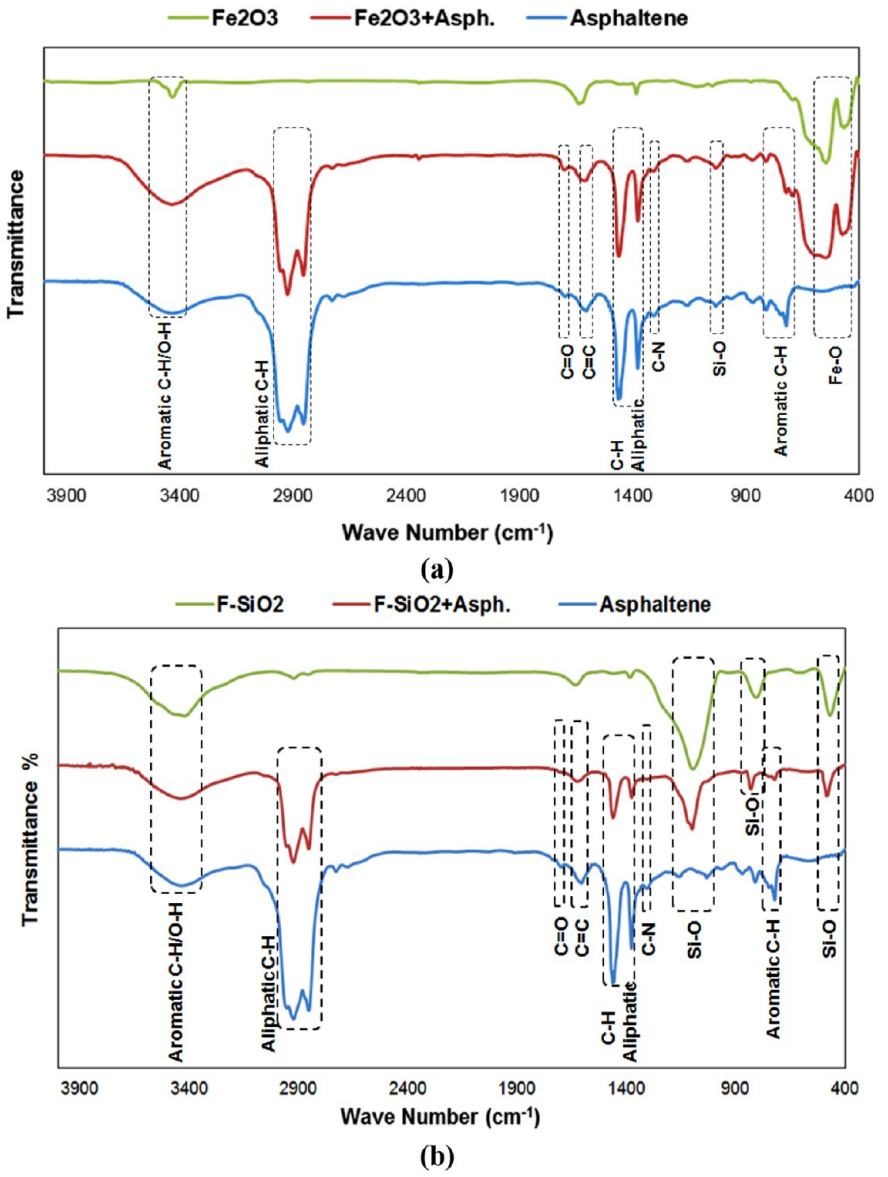

Figure 12. FTIR spectra of (a) pure asphaltenes, pure Fe_2O_3, and adsorbed asphaltenes onto the Fe_2O_3 and (b) pure asphaltenes, pure F-SiO_2, and adsorbed asphaltenes onto the F-SiO_2.

elimination of resins/maltenes occupying the cracks or gaps in the asphaltene structure. The elimination of created grooves/fractures in Figure 10g and h is contributed to the interactions of asphaltenes with nanoparticles acting as resin-like materials for stabilizing aggregated asphaltenes in the oil stream. Also, Figure 10g demonstrates that in the presence of Fe_2O_3 nanoparticles the gaps, grooves, or fractures are better occupied compared to the F-SiO_2 nanoparticles; this is in agreement with the results of SDS, HPM, and HPHT filtration experiments for higher asphaltene dispersion and inhibitory performance of Fe_2O_3 related to F-SiO_2. Comparison of the FESEM image in Figure 10g with h discloses that the sizes of asphaltene aggregates adsorbed onto the Fe_2O_3 nanoparticles are smaller than the sizes of aggregates on the surfaces of the F-SiO_2 nanoparticles. Thus, this explains the higher performance of the Fe_2O_3 nanoparticles for controlling the size growth of asphaltene aggregates.

3.5.2. TEM Analysis. TEM is particularly effective at providing a direct image of nanoaggregates and clusters in different asphaltene samples. Figure 11a, b, and c shows the TEM images of pure asphaltenes and adsorbed asphaltenes onto the Fe_2O_3 and F-SiO_2 nanoparticles, respectively. The images in the right column of Figure 11 show the close-up views of selected areas. Figure 11a demonstrates that purified asphaltene mainly consists of an irregular tangled structure with edges like a cauliflower, with an average size of 110−150 nm, in agreement with Perez-Hernandez et al. and AlHumaidan et al.[53,54] The observed tangled structure is ascribed to the existence of alkyl chains; these alkyl chains inhibit the complete stacking of aromatic sheets in asphaltene. The weak stacking of aromatic sheets causes an irregular and amorphous asphaltene structure which is obvious near the edge and in the inside of the sample. The mean distance between the stacking lines of aromatic sheets in purified asphaltene, referred to as mean interlayer spacing, is 0.385 nm as depicted in Figure 11a.

The TEM images in Figure 11b and c reveal that with addition of nanoparticles into the oil sample the size of

https://dx.doi.org/10.1021/acs.energyfuels.1c00060
Energy Fuels 2021, 35, 5908−5924

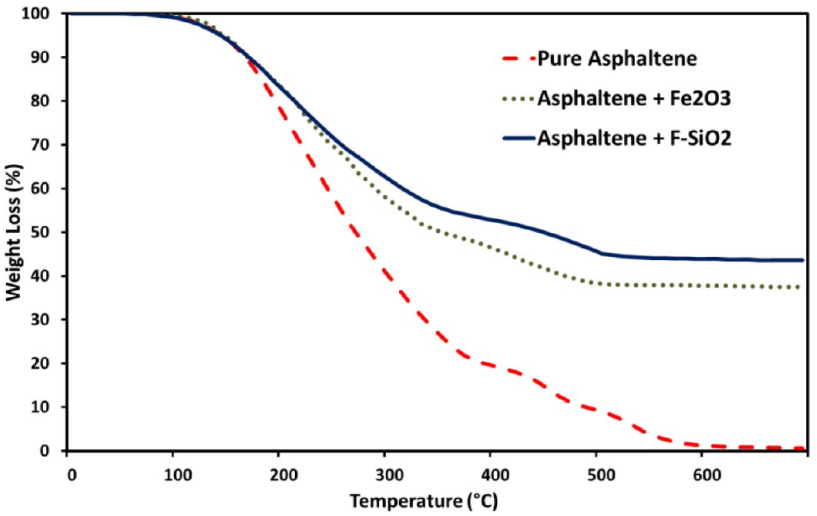

Figure 13. TGA mass loss curves of pure asphaltenes and asphaltenes adsorbed onto Fe_2O_3 and F-SiO_2 nanoparticles; asphaltenes were extracted from live oil after HPHT filtration experiments by the IP-143 method.

irregular tangled asphaltene structures is considerably decreased from 110−150 to about 40−80 nm. Furthermore, the mean interlayer spacing between aromatic sheets in the presence of Fe_2O_3 and F-SiO_2 nanoparticles increases from 0.385 to 0.470 and 0.442 nm, respectively. The decrease in asphaltene size and increase in mean interlayer spacing lead to the alteration of the asphaltene sample from unstable to stable as a consequence of attenuation of the $\pi-\pi$ stacking interaction between asphaltene molecules and establishment of strong interactions between nanoparticles and functional groups of asphaltene. These results are in line with the results obtained by FESEM.

3.5.3. FTIR Analysis. Here, the FTIR technique is used as the qualitative method for evaluation of functional groups of pure synthesized nanoparticles, solid asphaltenes, and adsorbed asphaltenes onto the surface of nanoparticles. The FTIR spectra of the analyzed materials are shown in Figure 12. For pure Fe_2O_3 (Figure 12a), the strong absorption peaks at 548 and 465 cm^{-1} can be attributed to the Fe−O band vibrations.[55] The weak absorption peak at 3418 cm^{-1} is assigned to the stretching and bending vibrations of the O−H bond which is an indication of a small amount of adsorbed water.[56] In the FTIR spectrum of F-SiO_2 in Figure 12b (green curve), two important absorption peaks around 1100 and 835 cm^{-1} are assigned to symmetric and asymmetric Si−O−Si stretching modes, respectively. As well, the peak near 460 cm^{-1} can be ascribed to the Si−O bending bond.[57] The absorption band at 3410 cm $^{-1}$ shows the presence of just a small amount of water which is recognized as the stretching vibration of either free O−H groups or free H_2O molecules.[56]

For pure asphaltenes, the obtained spectrum (Figure 12a and b, curve in blue) shows a C−H bond at 3415 cm^{-1} corresponding to a vibration in the aromatic double bonds (=C−H). It seems that the O−H groups have also been overlapped in this region. The two strong peaks at 2923 and 2853 cm^{-1} are detected in the regions for asymmetric aliphatic $C-H_3$ and $C-H_2$ stretching vibrations, respectively.[58] The low-intensity absorption band at around 1700 cm^{-1} is assigned to the stretching vibration of −C=O in the carboxyl groups.[59] The relatively weak peak at 1620 cm^{-1} is associated with stretching vibrations of C=C aromatic bonds.[60] The flexion bending mode of the CH_2 and CH_3 groups is responsible for the peaks at 1459 and 1378 cm^{-1}, respectively.[60] The weak peak at 1304 cm^{-1} corresponds to the C−N aromatic amine.[59]

The detected sharp peaks at 2923, 2853, 1459, and 1378 cm^{-1} in the spectrum of pure asphaltenes, as representative peaks, have been also observed for adsorbed asphaltenes onto the Fe_2O_3 and F-SiO_2 nanoparticles but with less intensity (red curve in Figure 12a and b). It confirms the full adsorption of asphaltenes onto the surfaces of synthesized nanoparticles. By comparison of the FTIR spectra of the adsorbed asphaltenes onto the surfaces of Fe_2O_3 and F-SiO_2 nanoparticles, the first feature worth commenting on is that the intensities of the observed peaks at 2923, 2853, 1459, and 1378 cm^{-1} for asphaltene-Fe_2O_3 are higher than the adsorbed asphaltenes onto the surface of F-SiO_2. It is also noticed that the absorption peaks at 548 and 465 cm^{-1} for Fe−O band vibrations have been more intensified in comparison to the weak absorption peak for the Si−O bending bond. Thus, more noticeable spectral changes are observed for the FTIR pattern of Fe_2O_3 nanoparticles after asphaltene adsorption. From these observations, it can be elucidated that more iron oxide nanoparticles were capped by asphaltenes, which confirms the much higher affinity of Fe_2O_3 for asphaltene adsorption than that of F-SiO_2. All these findings propose that ferrous oxide promotes the interaction of the nanoparticles with asphaltenes, which in principle agrees with the others' observations.[61,62]

3.5.4. TGA Analysis. The thermal stability or refractory nature of asphaltenes can be established by TGA with the measurement of weight loss. In addition, the amount of nanoparticles encapsulated into the asphaltene aggregates can be determined from the TGA data. TGA was carried out for asphaltene samples obtained from blank live oil and treated live oil with nanoparticles in HPHT filtration experiments to assess the adsorption of asphaltene aggregates onto the nanoparticles surfaces. The combustions of pure asphaltenes and asphaltenes adsorbed onto the surface of Fe_2O_3 and F-SiO_2 are presented in Figure 13.

On the basis of the TGA results, the thermal degradation of the studied pure asphaltene takes place in a single process with two main mass loss peaks (i.e., low and high temperature mass loss peaks), starting around 200 °C and ending at about 600 °C, with a residue content of less than 1% of the initial mass. This residue may consist of large aggregates of polycyclic

https://dx.doi.org/10.1021/acs.energyfuels.1c00060
Energy Fuels 2021, 35, 5908−5924

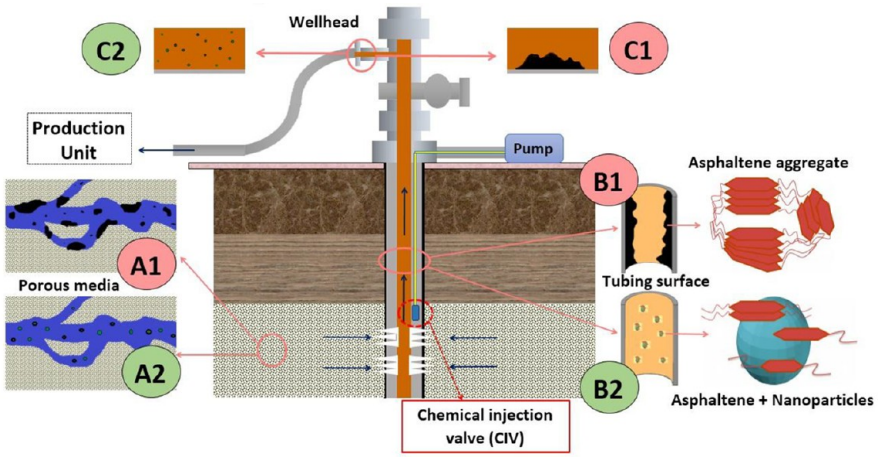

Figure 14. Schematic representation of some possible applications of the synthesized nanoparticles in oil industry. In A1 (surface of the reservoir rock in porous media), B1 (tubing surface in oil well), and C1 (flow line or connections of the wellhead assembly), the asphaltenes have deposited. By usage of the nanoparticles or nanofluids, asphaltene precipitation and deposition have been controlled in A2, B2, and C2. A2, B2, and C2 represent the states in which nanoparticles have been used.

condensed aromatic compounds and different elements such as V, Ni, and Fe that are stable at higher temperatures. The first step or low temperature mass loss peak is attributed to the degradation of aliphatic side chains (i.e., easily oxidized hydrocarbons); the second step or high temperature mass loss peak is associated to the degradation of the polynuclear aromatic sheets or the stacked layers as reported by others.[63,64]

Comparing the thermal profile of pure asphaltene (red curve) with the asphaltene adsorbed onto the nanoparticles shows that fully burning and the maximum weight loss temperature of asphaltene has decreased from 600 to about 500 °C. This shift in maximum weight loss temperature is attributed to the high adsorption of asphaltene on to the surfaces of the nanoparticles, which results in more asphaltene-accessible surface for burning. Consequently, it accelerates the asphaltene degradation/combustion process. The residue contents of the degradation process at the highest temperature in the presence of Fe_2O_3 and F-SiO_2 nanoparticles are about 38% and 44%, respectively. This residue content is more than the corresponding residue for the case of pure asphaltene (<1%). The largest fraction of the residue is the nanoparticles. Results of TGA also show that Fe_2O_3 nanoparticles can adsorb about 62% of asphaltenes (38% residue) which is more than the adsorbed asphaltenes by F-SiO_2 (about 56%). It proposes that much stronger intermolecular interactions occur between the adjacent molecules of Fe_2O_3 with asphaltenes such as hydrogen bonding, van der Waals, electrostatic, charge transfer, acid−base, and steric interactions. These data confirm the results obtained from FTIR analysis in Figure 12a and b. As a final point, similarities in the overall trend of the TGA curves in all cases show that no new or extra materials are formed because of the asphaltene−nanoparticle interactions. However, the nature and the structure of asphaltenes become less dense and softer when live oil is treated with the nanoparticles, concomitant with TEM results presented in Figure 11.

3.6. Implication of Experimental Results for Oil Field Applications. The synthesized nanoparticles, especially iron oxide (Fe_2O_3), are environmentally friendly and cost-effective materials with high potentials, which can be employed as the asphaltene inhibitor and dispersant to control the formation and growth of asphaltene particles in live oils at pressure and temperature conditions of oil fields. They can resolve operational issues induced by asphaltene in different sections of the oil industry. The possible applications of the synthesized nanoparticles are briefly discussed as follows.

The structural analyses of the synthesized nanoparticles by different techniques (BET, TEM, FESEM) have shown that the Fe_2O_3 and F-SiO_2 nanoparticles are uniform with average sizes in the range of 30−55 nm. The petrophysical−reservoir studies on different oil fields have established that the pore-throat radius of most reservoir rocks is in the range of 0.1−100 μm.[65,66] Hence, the synthesized nanoparticles can be easily injected in reservoir formations as an asphaltene inhibitor to postpone the onset pressure of asphaltene formation without pore-plugging concerns. The average sizes of the asphaltene aggregates in pressure and temperature ranges of oil wells, hydrocarbon flowlines, and production−refinery units are in a wide range from 10 nm to 15 μm.[28,67,68] Therefore, the mesoporous scale size of nanoparticles could be the optimum particles size for asphaltene adsorption. Consequently, the synthesized nanoparticles can be used in required sections as an efficient asphaltene dispersant to tackle the related problems. In Figure 14, applications of synthesized nanoparticles in different sections of an oil production system have been schematically illustrated. Without nanoparticles, asphaltene is deposited on reservoir rock/tubing surfaces and over the surface of the wellhead assemblies (A1, B1, and C1 in Figure 14). Injection of nanoparticles into the reservoir porous media and oil well (A2, B2, and C2) leads to the stabilization and dispersion of asphaltene in the bulk oil phase and thus prevents the plugging of porous media by the aggregation and growth of asphaltenes.

Mechanical methods, as the most current applied routines for treatment of asphaltene-related problems in oil fields, have negative points, as they are costly and unsafe due to technical risks such as tools stucking in the wells. Further, mechanical methods are inapplicable in the formation near the wellbore region with maximum asphaltene formation damage, and their usage requires stopping or disrupting the oil production. Thus, inhibition chemical strategies such as using nanoparticles at HPHT conditions are more attractive and advantageous approaches.

Implementation of synthesized nanoparticles in an oil production system requires uniform dispersion of synthesized

https://dx.doi.org/10.1021/acs.energyfuels.1c00060
Energy Fuels 2021, 35, 5908−5924

nanostructures in a base fluid to prepare the nanofluid. Considering that the oil is an organic compound, different types of organic base fluid or solvents such as aromatics and common petroleum products can be used for preparation of the desired nanofluids. For production tubing or porous media applications, the nanofluid can be injected by coil tubing or injection pumps through the chemical injection valves installed on appropriate points. For injection of nanofluids into the porous media, the altered or damaged zone (i.e., effective wellbore radius or skin radius) near the wellbore should be determined. The effective wellbore radius and the method of injection (continuous or batchwise) require core-flood experiments at pressure and temperature conditions of operation. As well, recent studies propose in situ synthesis of nanoparticles in the oil medium by the aid of asphaltenes as the oil indigenous surfactants.[69,70] This method should be further evaluated at operational conditions as an injection scenario for chemical inhibition or dispersion of asphaltene precipitation in porous media. For selection and design of base fluid, economical and environmental concerns should be taken into consideration. In addition, the stability or complete dispersion of nanoparticles in a base fluid is an important challenging matter faced by different industries. To avoid the sedimentation of nanoparticles during its operation, efficient surfactants may be added to the base fluid.

4. CONCLUSIONS

In this study, Fe_2O_3 and functionalized SiO_2 (F-SiO_2) nanoparticles were synthesized to assess their potential applications for controlling formation and growth of asphaltenes in an unstable live oil at high pressures and temperature of oil field conditions. In the presence of Fe_2O_3 and F-SiO_2 nanoparticles, the studied live oil remains more stable, and the onset of asphaltene precipitation has been delayed during isothermal depressurization. However, the performance of Fe_2O_3 in the control of asphaltene precipitation and aggregation is much higher than the F-SiO_2 nanoparticles. The average sizes of asphaltene aggregates by HPM and the amount of precipitated asphaltenes by HPHT filtration at different pressure steps and a temperature of 274.9 °F are in decreasing order of (blank oil + Fe_2O_3) < (blank oil + F-SiO_2) < (blank oil). TEM analyses demonstrate that the addition of nanoparticles to the live oil leads to reduction of the size of irregular tangled asphaltene structures from 110 to 150 nm to about 40−80 nm. Considering the average size of the pore-throat radius of most reservoir rocks, pore-plugging concerns of asphaltene in porous media can be resolved. The decrease in the asphaltene aggregate size and increase in the mean interlayer spacing of the asphaltene aromatic sheets alter the unstable asphaltene sample to be stable due to the attenuation of the $\pi-\pi$ stacking interaction between asphaltene molecules and establishment of strong nanoparticle−asphaltene interactions. Compared to F-SiO_2, Fe_2O_3 nanoparticles exhibit a higher potential to interact with the asphaltenes and help stabilize them in the oil phase. Obtained results from HPHT experiments are well justified with analysis of intermolecular interactions by FESEM, FTIR, and TGA. Findings of this study demonstrate that Fe_2O_3 nanoparticles can serve as an excellent asphaltene inhibitor and dispersant for stabilizing asphaltenes in live oil with controlling the rate of asphaltene aggregation at HPHT.

■ ASSOCIATED CONTENT

Supporting Information

The Supporting Information is available free of charge at https://pubs.acs.org/doi/10.1021/acs.energyfuels.1c00060.

Procedure for determination of optimum dosage of nanoparticles for high pressure−high temperature experiments(PDF)

■ AUTHOR INFORMATION

Corresponding Authors

Negahdar Hosseinpour − *Institute of Petroleum Engineering (IPE), University of Tehran, Tehran, Iran;* orcid.org/0000-0002-6325-0758; Email: nhosseinpour@ut.ac.ir

Saber Mohammadi − *Petroleum Engineering Department, Research Institute of Petroleum Industry (RIPI), Tehran, Iran;* orcid.org/0000-0002-2919-6719; Email: mohammadi.sab@gmail.com; Fax: +98-21-44739746

Authors

Fatemeh Mahmoudi Alemi − *Petroleum Engineering Department, Research Institute of Petroleum Industry (RIPI), Tehran, Iran;* orcid.org/0000-0002-1555-6891

Seyed Ali Mousavi Dehghani − *Petroleum Engineering Department, Research Institute of Petroleum Industry (RIPI), Tehran, Iran;* orcid.org/0000-0003-2268-9884

Ali Rashidi − *School of Chemistry, University of Tehran, Tehran, Iran*

Complete contact information is available at: https://pubs.acs.org/10.1021/acs.energyfuels.1c00060

Notes

The authors declare no competing financial interest.

■ ACKNOWLEDGMENTS

The authors greatly acknowledge the Petroleum Engineering Department of the Research Institute of Petroleum Industry (RIPI) for providing HPHT experimental assemblies.

■ REFERENCES

(1) Peng, B.; Tang, J.; Luo, J.; Wang, P.; Ding, B.; Tam, K. C. Applications of Nanotechnology in Oil and Gas Industry: Progress and Perspective. *Can. J. Chem. Eng.* **2018**, *96*, 91−100.

(2) Agista, M.; Guo, K.; Yu, Z. State-Of-The-Art Review of Nanoparticles Application in Petroleum with a Focus on Enhanced Oil Recovery. *Appl. Sci.* **2018**, *8*, 871.

(3) Shakib, J. T.; Kanani, V.; Pourafshary, P. Nano-clays as Additives for Controlling Filtration Properties of Water−Bentonite Suspensions. *J. Pet. Sci. Eng.* **2016**, *138*, 257−264.

(4) Ahmad, H. M.; Kamal, M. S.; Murtaza, M.; Al-Harthi, M. A. Improving the Drilling Fluid Properties Using Nanoparticles and Water-Soluble Polymers. *SPE Kingdom of Saudi Arabia Annual Technical Symposium and Exhibition*, Dammam, Saudi Arabia, 24−27 April 2017; SPE-188140.

(5) Al-Muntasheri, G. A.; Liang, F.; Hull, K. L. Nanoparticle-Enhanced Hydraulic-Fracturing Fluids: A Review. *SPE Prod. Oper.* **2017**, *32*, 186−195.

(6) Bahatia, K. H.; Chacko, L. P. Ni-Fe Nanoparticle: An Innovative Approach for Recovery of Hydrates. *Brasil Offshore*, Macaé, Brazil, 14−17 June 2011; SPE-143159.

(7) Liu, T.; Jiang, G.; Zhang, P.; Sun, J.; Sun, H.; Wang, R.; Zheng, M. A New Low-Cost Drilling Fluid for Drilling in Natural Gas Hydrate-Bearing Sediments. *J. Nat. Gas Sci. Eng.* **2016**, *33*, 934−941.

(8) Liu, P.; Li, X.; Yu, H.; Niu, L.; Yu, L.; Ni, D.; Zhang, Z. Functional Janus-SiO_2 Nanoparticles Prepared by a Novel "Cut the Gordian Knot" Method and Their Potential Application for Enhanced Oil Recovery. *ACS Appl. Mater. Interfaces* **2020**, *12*, 24201−24208.
(9) Maghzi, A.; Mohammadi, S.; Ghazanfari, M. H.; Kharrat, R.; Masihi, M. Monitoring Wettability Alteration by Silica Nanoparticles During Water Flooding to Heavy Oils in Five-Spot Systems: A Pore-Level Investigation. *Exp. Therm. Fluid Sci.* **2012**, *40*, 168−176.
(10) Radnia, H.; Rashidi, A.; Solaimany Nazar, A. R.; Eskandari, M. M.; Jalilian, M. A Novel Nanofluid Based on Sulfonated Graphene for Enhanced Oil Recovery. *J. Mol. Liq.* **2018**, *271*, 795−806.
(11) Zhou, Y.; Wu, X.; Zhong, X.; Sun, W.; Pu, H.; Zhao, J. X. Surfactant-Augmented Functional Silica Nanoparticle Based Nanofluid for Enhanced Oil Recovery at High Temperature and Salinity. *ACS Appl. Mater. Interfaces* **2019**, *11*, 45763−45775.
(12) Bayat, A. E.; Junin, R.; Samsuri, A.; Piroozian, A.; Hokmabadi, M. Impact of Metal Oxide Nanoparticles on Enhanced Oil Recovery from Limestone Media at Several Temperatures. *Energy Fuels* **2014**, *28*, 6255−6266.
(13) Druetta, P.; Picchioni, F. Polymer and Nanoparticles Flooding as a New Method for Enhanced Oil Recovery. *J. Pet. Sci. Eng.* **2019**, *177*, 479−495.
(14) Pereira, L. O. M.; Maia, K. C. B.; Silva, W. C.; Leite, A. C.; Francisco, A. D. S.; Vasconcelos, T. L.; Nascimento, R. S. V.; Grasseschi, D. Fe_3O_4 Nanoparticles as Surfactant Carriers for Enhanced Oil Recovery and Scale Prevention. *ACS Appl. Nano Mater.* **2020**, *3*, 5762−5772.
(15) Nassar, N. N. Asphaltene Adsorption onto Alumina Nanoparticles: Kinetics and Thermodynamic Studies. *Energy Fuels* **2010**, *24*, 4116−4122.
(16) Mohammadi, M.; Akbari, M.; Fakhroueian, Z.; Bahramian, A.; Azin, R.; Arya, Sh. Inhibition of Asphaltene Precipitation by TiO_2, SiO_2, and ZrO_2 Nanofluids. *Energy Fuels* **2011**, *25*, 3150−3156.
(17) Hosseinpour, N.; Khodadadi, A. A.; Bahramian, A.; Mortazavi, Y. Asphaltene Adsorption onto Acidic/Basic Metal Oxide Nanoparticles Toward In Situ Upgrading of Reservoir Oils by Nanotechnology. *Langmuir* **2013**, *29*, 14135−14146.
(18) Kazemzadeh, Y.; Eshraghi, E.; Kazemi, K.; Sourani, S.; Mehrabi, M.; Ahmadi, Y. Behavior of Asphaltene Adsorption onto the Metal Oxide Nanoparticle Surface and its Effect on Heavy Oil Recovery. *Ind. Eng. Chem. Res.* **2015**, *54*, 233−239.
(19) Shojaati, F.; Riazi, M.; Mousavi, S. H.; Derikvand, Z. Experimental Investigation of the Inhibitory Behavior of Metal Oxides Nanoparticles on Asphaltene Precipitation. *Colloids Surf., A* **2017**, *531*, 99−110.
(20) Ezeonyeka, N. L.; Hemmati-Sarapardeh, A.; Husein, M. M. Asphaltenes Adsorption onto Metal Oxide Nanoparticles: A Critical Evaluation of Measurement Techniques. *Energy Fuels* **2018**, *32*, 2213−2223.
(21) Hammami, A.; Ratulowski, J. Precipitation and Deposition of Asphaltenes in Production Systems: A Flow Assurance Overview. In *Asphaltenes, Heavy Oils, and Petroleomics*; Mullins, O. C., Sheu, E. Y., Hammami, A., Marshall, A. G., Eds.; Springer, New York, 2007; pp 617−660.
(22) Fakher, Sh.; Ahdaya, M.; Elturki, M.; Imqam, A. Critical Review of Asphaltene Properties and Factors Impacting its Stability in Crude Oil. *J. Pet. Explor. Prod. Technol.* **2020**, *10*, 1183−1200.
(23) Durand, E.; Clemancey, M.; Lancelin, J. M.; Verstraete, J.; Espinat, D.; Quoineaud, A. A. Effect of Chemical Composition on Asphaltenes Aggregation. *Energy Fuels* **2010**, *24*, 1051−1062.
(24) Cao, M.; Gu, Y. Oil Recovery Mechanisms and Asphaltene Precipitation Phenomenon in Immiscible and Miscible Co Flooding Processes. *Fuel* **2013**, *109*, 157−166.
(25) Nassar, N. N.; Hassan, A.; Pereira-Almao, P. Metal Oxide Nanoparticles for Asphaltene Adsorption and Oxidation. *Energy Fuels* **2011**, *25*, 1017−1023.
(26) Taborda, E. E.; Franco, C. A.; Lopera, S. H.; Alvarado, V.; Cortés, F. B. Effect of Nanoparticles/Nanofluids on the Rheology of Heavy Crude Oil and its Mobility on Porous Media at Reservoir Conditions. *Fuel* **2016**, *184*, 222−232.
(27) López, D.; Giraldo, L. J.; Lucas, E. F.; Riazi, M.; Franco, C. A.; Cortés, F. B. Cardanol/SiO_2 Nanocomposites for Inhibition of Formation Damage by Asphaltene Precipitation/Deposition in Light Crude Oil Reservoirs. Part I: Novel Nanocomposite Design Based on SiO_2−Cardanol Interactions. *Energy Fuels* **2020**, *34*, 7048−7057.
(28) Joshi, N. B.; Mullins, O. C.; Jamaluddin, A.; Creek, J.; McFadden, J. Asphaltene Precipitation from Live Crude Oil. *Energy Fuels* **2001**, *15*, 979−86.
(29) Ahmadi, Y.; Aminshahidy, B. Effects of Hydrophobic CaO and SiO_2 Nanoparticles on Asphaltene Precipitation Envelope (APE): An Experimental and Modeling Approach. *Oil Gas Sci. Technol.* **2018**, *73*, 56.
(30) Kabir, C. S.; Jamaluddin, A. K. M. Asphaltene Characterization and Mitigation in South Kuwait's Marrat Reservoir. *SPE Middle East Oil Show*, Bahrain, 20−23 February 1999; SPE-53155.
(31) Leontaritis, K. J.; Mansoori, G. A. Asphaltene Deposition: A Survey of Field Experiences and Research Approaches. *J. Pet. Sci. Eng.* **1988**, *1*, 229−239.
(32) Reudelhuber, F. O. Sampling Procedure for Oil Reservoirs. *JPT, J. Pet. Technol.* **1957**, *9*, 15−18.
(33) Aquino-Olivos, M. A.; Buenrostro-Gonzalez, E.; Andersen, S. I.; Lira-Galeana, C. Investigations of Inhibition of Asphaltene Precipitation at High Pressure Using Bottomhole Samples. *Energy Fuels* **2001**, *15*, 236−240.
(34) Hammami, A.; Phelps, C. H.; Monger-McClure, T.; Little, T. M. Asphaltene Precipitation from Live Oils: An Experimental Investigation of Onset Conditions and Reversibility. *Energy Fuels* **2000**, *14*, 14−18.
(35) Engel, D.; Azevedo, V.; Pontes, T. Improvements to Data Acquisition and Bottomhole Fluid Sampling in Offshore Drill-Stem Testing. *SPE Latin America and Caribbean Petroleum Engineering Conference*, Maracaibo, Venezuela, 21−23 May 2014; SPE1-69477.
(36) *ASTM D2007-91: Standard Test Method for Characteristic Groups in Rubber Extender and Processing Oils and Other Petroleum-Derived Oils by the Clay-Gel Absorption Chromatographic Method*; Book of Standards 5.01; American Society for Testing and Materials, Philadelphia, PA, 1993.
(37) Yen, A.; Yin, Y. R.; Asomaning, S. Evaluating Asphaltene Inhibitors: Laboratory Tests and Field Studies. *SPE International Symposium on Oilfield Chemistry*, Houston, Texas, 13−16 February 2001; SPE-65376.
(38) Pereira, V. J.; Setaro, L. L. O.; Costa, G. M. N.; Vieira de Melo, S. A. B. Evaluation and Improvement of Screening Methods Applied to Asphaltene Precipitation. *Energy Fuels* **2017**, *31*, 3380−3391.
(39) De Boer, R. B.; Leerlooyer, K.; Eigner, M. R. P.; Van Bergen, A. R. D. Screening of Crude Oils for Asphalt Precipitation: Theory, Practice, and the Selection of Inhibitors. *SPE Prod. Facil.* **1995**, *10*, 55−61.
(40) Mohammadi, S.; Rashidi, F.; Mousavi-Dehghani, S. A.; Ghazanfari, M. H. Reversibility of Asphaltene Aggregation in Live Oils: Qualitative and Quantitative Evaluation. *J. Chem. Eng. Data* **2015**, *60*, 2646−2654.
(41) Collins, T. J. ImageJ for Microscopy. *BioTechniques* **2007**, *43*, S25−S30.
(42) Mousavi Dehghani, S. A.; Sefti, M. V.; Mansoori, G. A. Simulation of Natural Depletion and Miscible Gas Injection Effects on Asphaltene Stability in Petroleum Reservoir Fluids. *Pet. Sci. Technol.* **2007**, *25*, 1435−1446.
(43) Mohammadi, S.; Rashidi, F.; Mousavi-Dehghani, S. A.; Ghazanfari, M. H. On the Effect of Temperature on Precipitation and Aggregation of Asphaltenes in Light Live Oils. *Can. J. Chem. Eng.* **2016**, *94*, 1820−1829.
(44) *ASTM D3279-90: Standard Test Method for Determination of Asphaltenes (Heptane Insolubles) in Crude Petroleum and Petroleum Products*; Book of Standards 04.03; American Society for Testing and Materials, Philadelphia, PA, , 1985.

https://dx.doi.org/10.1021/acs.energyfuels.1c00060
Energy Fuels 2021, 35, 5908−5924

(45) Fard, S. R.; Khadar, R. H. The Effect of Inhibitors Asphaltene Precipitation Due to a Natural Depletion Mechanism in Crude Oil. *Energy Sources, Part A* **2012**, *34*, 1868−1875.
(46) Firoozinia, H.; Fouladi Hossein Abad, K.; Varamesh, A. A Comprehensive Experimental Evaluation of Asphaltene Dispersants for Injection under Reservoir Conditions. *Pet. Sci.* **2016**, *13*, 280−291.
(47) Lhuissier, M.; Couvert, A.; Amrane, A.; Kane, A.; Audic, J. L. Characterization and Selection of Waste Oils for the Absorption and Biodegradation of VOC of Different Hydrophobicities. *Chem. Eng. Res. Des.* **2018**, *138*, 482−489.
(48) Díaz-Díez, M. A.; Gómez-Serrano, V.; Fernández González, C.; Cuerda-Correa, E. M.; Macías-García, A. Porous Texture of Activated Carbons Prepared by Phosphoric Acid Activation of Woods. *Appl. Surf. Sci.* **2004**, *238*, 309−313.
(49) Igder, M.; Hosseinpour, N.; Biyouki, A. A.; Bahramian, A. Control of Asphaltenes Aggregation in Reservoir Model Oils along Production Streamline by Fe_3O_4 and NiO Nanoparticles. *Energy Fuels* **2018**, *32*, 6689−6697.
(50) Bogatyrev, V.M.; Gun'ko, V.M.; Galaburda, M.V.; Borysenko, M.V.; Pokrovskiy, V.A.; Oranska, O.I.; Polshin, E.V.; Korduban, O.M.; Leboda, R.; Skubiszewska-Zieba, J. Synthesis and Characterization of Fe_2O_3/SiO_2 Nanocomposites. *J. Colloid Interface Sci.* **2009**, *338*, 376−388.
(51) Nikmah, A.; Taufiq, A.; Hidayat, A. Synthesis and Characterization of Fe_3O_4/SiO_2 Nanocomposites; *IOP Conference Series: Earth and Environmental Science, International Conference on Life Sciences and Technology*, Malang, Indonesia, Vol. *276*, 4 September 2018.
(52) Groenzin, H.; Mullins, O. C. Molecular Size and Structure of Asphaltenes from Various Sources. *Energy Fuels* **2000**, *14*, 677−684.
(53) Perez-Hernandez, R.; Mendoza-Anaya, D.; Mondragon-Galicia, G.; Espinosa, M.; Rodriguez-Lugo, V.; Lozada, M.; Arenas-Alatorre, J. Microstructural Study of Asphaltene Precipitated with Methylene Chloride and n-Hexane. *Fuel* **2003**, *82*, 977−982.
(54) AlHumaidan, F. S.; Rana, M. S.; Tanoli, N. J.; Lababidi, H. M. S.; Al-Najdi, N. A. Changes in Asphaltene Surface Topography with Thermal Treatment. *Arabian J. Chem.* **2020**, *13*, 5377−5389.
(55) Liu, H.; Li, P.; Lu, B.; Wei, Y.; Sun, Y. Transformation of Ferrihydrite in the Presence or Absence of Trace Fe(II): the Effect of Preparation Procedures of Ferrihydrite. *J. Solid State Chem.* **2009**, *182*, 1767−1771.
(56) Darezereshki, E. One-Step Synthesis of Hematite (a-Fe_2O_3) Nano-Particles by Direct Thermal-Decomposition of Maghemite. *Mater. Lett.* **2011**, *65*, 642−645.
(57) Samitier, J.; Marco, S.; Ruiz, o.; Morante, J. R.; Esteve-Tinto, J.; Bausells, J. Analysis by FT-IR Spectroscopy of SiO_2-Polycrystalline Structures Used in Micromechanics: Stress Measurements. *Sens. Actuators, A* **1992**, *32*, 347−353.
(58) Chen, Y.; Wang, Y.; Lu, J.; Wu, C. The Viscosity Reduction of Nano-Keggin-K3PMo12O40 in Catalytic Aquathermolysis of Heavy Oil. *Fuel* **2009**, *88*, 1426−1434.
(59) Wang, Y.; Xia, T. D.; Zheng, H.; Feng, H. X. Stearic Acid/Silica Fume Composite as Form-Stable Phase Change Material for Thermal Energy Storage. *Energy Buil.* **2011**, *43*, 2365−2370.
(60) Parra-Barraza, H.; Hernandez-Montiel, D.; Lizardi, J.; Hernandez, J.; Herrera Urbina, R.; Valdez, M. A. The Zeta Potential and Surface Properties of Asphaltenes Obtained with Different Crude Oil/nheptane Proportions. *Fuel* **2003**, *82*, 869−874.
(61) Abdullah, M. M. S.; Al-Lohedan, H. A.; Atta, A. M. Novel Magnetic Iron Oxide Nanoparticles Coated with Sulfonated Asphaltene as Crude Oil Spill Collectors. *RSC Adv.* **2016**, *6*, 59242−59249.
(62) Carbognani, L. Effects of Iron Compounds on the Retention of Oil Polar Hydrocarbons over Solid Sorbents. *Pet. Sci. Technol.* **2000**, *18*, 335−360.
(63) Maity, K.; Blanco, E.; Ancheyta, J.; Alonso, F.; Fukuyama, H. Early Stage Deactivation of Heavy Crude Oil Hydroprocessing Catalysts. *Fuel* **2012**, *100*, 17−23.
(64) Hosseinpour, N.; Mortazavi, Y.; Bahramian, A.; Khodatars, L.; Khodadadi, A. A. Enhanced Pyrolysis and Oxidation of Asphaltenes Adsorbed onto Transition Metal Oxides Nanoparticles Towards Advanced In-situ Combustion EOR Processes by Nanotechnology. *Appl. Catal., A* **2014**, *477*, 159−171.
(65) Kashif, M.; Cao, Y.; Yuan, G.; Asif, M.; Javed, K.; Mendez, J. N.; Khan, D.; Miruo, L. Pore Size Distribution, Their Geometry and Connectivity in Deeply Buried Paleogene Es1 Sandstone Reservoir, Nanpu Sag, East China. *Pet. Sci.* **2019**, *16*, 981−1000.
(66) Ismail, A.; Yasin, Q.; Du, Q. Application of Hydraulic Flow Unit for Pore Size Distribution Analysis in Highly Heterogeneous Sandstone Reservoir: A Case Study. *J. Jpn. Pet. Inst.* **2018**, *61*, 246−255.
(67) Mohammadi, S.; Rashidi, F.; Mousavi-Dehghani, S. A.; Ghazanfari, M. H. Modeling of Asphaltene Aggregation Phenomena in Live Oil Systems at High Pressure-High Temperature. *Fluid Phase Equilib.* **2016**, *423*, 55−73.
(68) Mullins, O. C.; Seifert, D. J.; Zuo, J. Y.; Zeybek, M. Clusters of Asphaltene Nanoaggregates Observed in Oilfield Reservoirs. *Energy Fuels* **2013**, *27*, 1752−1761.
(69) Amrollahi Biyouki, A.; Hosseinpour, N.; Bahramian, A.; Vatani, A. In-situ Upgrading of Reservoir Oils by In-Situ Preparation of NiO Nanoparticles in thermal Enhanced Oil Recovery Processes. *Colloids Surf., A* **2017**, *520*, 289−300.
(70) Amrollahi Biyouki, A.; Hosseinpour, N.; Nassar, N. N. Pyrolysis and Oxidation of Asphaltene-Born Coke-like Residue Formed onto in Situ Prepared NiO Nanoparticles toward Advanced in Situ Combustion Enhanced Oil Recovery Processes. *Energy Fuels* **2018**, *32*, 5033−5044.

https://dx.doi.org/10.1021/acs.energyfuels.1c00060
Energy Fuels 2021, 35, 5908−5924